Biochimie 93 (2011) 1328–1340

Contents lists available at ScienceDirect

Biochimie

journal homepage: www.elsevier.com/locate/biochi

Research paper

Naphthalene diimide scaffolds with dual reversible and covalent interaction properties towards G-quadruplex

Matteo Nadai [b], Filippo Doria [a], Marco Di Antonio [c], Giovanna Sattin [b], Luca Germani [a], Claudia Percivalle [a], Manlio Palumbo [c], Sara N. Richter [b,*], Mauro Freccero [a,**]

[a] Dipartimento di Chimica, Università di Pavia, V.le Taramelli 10, 27100 Pavia, Italy
[b] Dipartimento di Istologia, Microbiologia e Biotecnologie Mediche, via Gabelli 63, 35121 Padova, Italy
[c] Dipartimento di Scienze Farmaceutiche, Università di Padova, Via Marzolo 5, 35131 Padova, Italy

ARTICLE INFO

Article history:
Received 1 March 2011
Accepted 14 June 2011
Available online 16 June 2011

Keywords:
DNA
G-quadruplex
Recognition
Alkylation
Selectivity
Quinone methide

ABSTRACT

Selective recognition and alkylation of G-quadruplex oligonucleotides has been achieved by substituted naphthalene diimides (NDIs) conjugated to engineered phenol moieties by alkyl-amido spacers with tunable length and conformational mobility. FRET-melting assays, circular dichroism titrations and gel electrophoresis analysis have been carried out to evaluate both reversible stabilization and alkylation of the G-quadruplex. The NDIs conjugated to a quinone methide precursor (NDI-QMP) and a phenol moiety by the shortest alkyl-amido spacer exhibited a planar and fairly rigid geometry (modelled by DFT computation). They were the best irreversible and reversible G-quadruplex binders, respectively. The above NDI-QMP was able to alkylate the telomeric G-quadruplex DNA in the nanomolar range and resulted 100–1000 times more selective on G-quadruplex versus single- and double-stranded oligonucleotides. This compound was also the most cytotoxic against a lung carcinoma cell line.

1. Introduction

Guanine rich oligonucleotides are capable of folding into supramolecular structures called G-quadruplex (G-4) [1]. In more detail, a planar tetrameric arrangement of guanines (G-tetrad), stabilized by hydrogen bonding, can self-aggregate by π-stacking interactions and monovalent cation coordination (i.e Na^+ and K^+), generating a G-4 [2]. Due to the molecular complexity of the above, a large number of topologically different G-4 structures can be formed depending on strand stoichiometry, strand orientation and guanosine relative conformation [3–5]. In some cases different monovalent cations could also lead the same oligonucleotide sequence to fold into different G-4 topologies [6]. G-4 topologies have been described as parallel, antiparallel or mixed-type, depending on the direction of the G-4 forming strands. Beside these supramolecular aspects, the growing interest on G-4 is justified by their potential implication in biological processes crucial for genomic stability, such as transcription of oncogenes and translation of the related mRNA [7–13]. Moreover, it has been demonstrated that addition of efficient G-4 ligands in-*cellulo* affects the binding affinity of some proteins, such as SP-1 and Shelterin, towards specific region of the genome [14–16]. Displacement of the above proteins activates DNA damage responses and eventually triggers biological pathways which lead to cell apoptosis or senescence.

Indeed, it has been shown that stabilization of G-4 folded structures by small molecules or selective antibodies is responsible for oncogenes down regulation in-*vitro* (i.e *Bcl-2*, *c-myc*) and telomerase inhibition [17–24]. Since telomerase induces telomere elongation and hence is required for immortalization of the tumour cells, the above strategy could be exploited for the development of new selective antitumour drugs [25]. More recently, also G-4 RNA has been shown to behave as translational switch *in-vitro*, broadening the interest for such structures as tools for unravelling biological processes regulation at the molecular level [26].

Because of all these reasons, a large number of G-4 selective ligands has been reported to date [27,28]. The common features shared among a large number of these compounds are: the potential for a flat conformation, the presence of an electron poor aromatic core and cationic or protonable moieties. These characteristics can be modulated in order to improve the specific

* Corresponding author. Tel.: +390498272346; fax: +390498272355.
** Corresponding author. Tel.: +390382987768; fax: +390382987323.
E-mail addresses: sara.richter@unipd.it (S.N. Richter), mauro.freccero@unipv.it (M. Freccero).

0300-9084/$ – see front matter © 2011 Elsevier Masson SAS. All rights reserved.
doi:10.1016/j.biochi.2011.06.015

recognition (i) of quadruplex over duplex-DNA and (ii) between different G-4 sequences and topologies. Particularly promising from this point of view are the synthetic molecules Braco-19 [29], the related acridines [30], pyridine-2,6-dicarboxylic acid bis-quinolin-2-ylamides (PDCs) [16] and quinolinium analogues [31,32], as well as the natural product Telomestatin [33] and synthetic related structures [34]. A series of naphthalene diimide derivatives (NDIs) have also been described. In more detail, disubstituted NDIs showed low selectivity for G-4 [35], while tri- and tetra-substituted NDIs exhibited high G-4 affinity [36,37], with noteworthy selectivity for the parallel topology [38,39]. All the described agents act as reversible G-4 ligands. Our group has recently developed NDI derivatives coupled to *ortho*-quinone methides (*o*-QMs), which are potent and transient reactive electrophilies [40–42], paving the route for the generation of new G-4 covalent ligands [43]. *o*-QM have to be generated by activation of suitable quinone methide precursors (QMPs), under biocompatible conditions, such as: mild thermal digestion (40 °C) [40,44–46], UV–Vis irradiation [47–51] and mild mono-electronic reduction [44]. The conjugated NDI-QMPs in Scheme 1 may act as hybrid ligand-alkylating structures selectively targeting G-4 folding oligonucleotides [52]. Their analogues, lacking the reactive moiety $CH_2NMe_3^+$, behave as reversible ligands (**NDI-AminoPhenol**, in Scheme 1).

All of the NDI-QMPs developed so far, present a quaternary ammonium moiety (NMe_3^+) as good leaving group for mild QM generation (Scheme 1). Such a key structural feature also represents an important limiting factor in terms of cells permeability and biological applications, hampering their potential pharmacological applications. We herein describe a second generation NDI-QMP hybrids in which a neutral *o*-hydroxy benzyl alcohol moiety function as QMP (Scheme 2).

Due to the alkylation selectivity towards G-4 folded oligonucleotide showed by NDIs **1**–**6** in the biophysical assays herein reported, we believe that such a class of ligands, could be further exploited for unravelling new G-4 related biological processes as well as a genome wide screening of new relevant G-4 structures. Their G-4 selectivity is prompted by the good reversible binding properties.

Here we briefly describe the synthesis and the bioassays of a small library of the tri-substituted NDI ligands **1**–**6** and **1a**–**4a**, as G-4 selective hybrid ligand/alkylating compounds and reversible ligands, respectively (Scheme 2).

2. Materials and methods

2.1. Chemical synthesis

The amines 2-amino-N-(4-hydroxyphenyl)acetamide (**11**) and 3-amino-N-(4-hydroxyphenyl)propanamide (**12**) have been synthesized according to an original synthetic protocol, described in the Supporting information. The compound **13** has been synthesized by a three-step synthetic protocol starting from 2-(bromomethyl)-4-nitrophenol (see Supporting information for details).

2-chloro-N-(2,2-dimethyl-4H-benzo[d][1,3]dioxin-6-yl)acetamide (14): The isopropylidenacetal (**13**) 500 mg (2.78 mmol) was dissolved in 15 ml of dry THF followed by the addition of 1 ml of TEA at 0 °C. Chloroacetyl chloride (0.4 ml, 5.0 mmol) was added dropwise under vigorous stirring, keeping the temperature at 0 °C. The resulting solution was stirred at 0 °C for 2 h. Reaction mixture was quenched by adding 10 ml of ethyl acetate. The resulting suspension was washed twice with a $NaHCO_3$ solution. The organic layers were collected, dried on Na_2SO_4 and the solvent was evaporated under vacuum, affording the 2-chloro-N-(4-hydroxyphenyl) acetamide as a brown solid, which was purified by flash chromatography (cycloesane:ethyl acetate 8:2). Yield 93%. ^{1}H NMR (300 MHz, $CDCl_3$, 25 °C, TMS): $\delta = 8.2$ (s, 1H), 7.25 (d, 1H, $J = 2.4$ Hz), 7.05 (dd, 1H, $J = 2.4$ Hz, $J = 8.7$ Hz), 6.8 (d, 1H, $J = 8.7$ Hz), 4.8 (s, 2H), 4.10 (s, 2H), 1.55 (s, 6H). ^{13}C NMR (300 MHz, $CDCl_3$): $\delta = 163.7, 148.5, 129.4, 120.6, 119.7, 117.3, 117.0, 99.5, 60.7, 40.6, 24.5$. Anal. Calcd. for $C_{12}H_{14}NO_3Cl$: C, 56.37; H, 5.52; Cl, 13.87; N, 5.48; O, 18.77. Found: C, 56.51; H, 5.47; N, 5.41.

3-chloro-N-(2,2-dimethyl-4H-benzo[d][1,3]dioxin-6-yl) propanamide (15): $NaHCO_3$ (250 mg) was added to a CH_3CN solution (15 ml) of 3-chloropropionyl chloride (0.34 ml, 3.6 mmol), keeping the temperature at 0 °C. 2-(hydroxymethyl)-4-amino isopropylidenacetal (**13**) (500 mg 1.8 mmol) in 15 ml of CH_3CN was added dropwise to the suspension and stirred for 2 h. 20 ml of aqueous $NaHCO_3$ were added to the mixture and the CH_3CN was removed under reduced pressure. $CHCl_3$ extraction (3 × 50 ml) of the resulting aqueous solution afforded the product as a brown oil, which has been used in the next step without further purification. 78% Yield.

4-chloro-N-(2,2-dimethyl-4H-benzo[d][1,3]dioxin-6-yl)butanamide (16): 4-Chlorobutyryl chloride (0.47 ml, 4.18 mmol) dissolved in 15 ml of DMA has been treated with 260 mg $NaHCO_3$ at r.t.

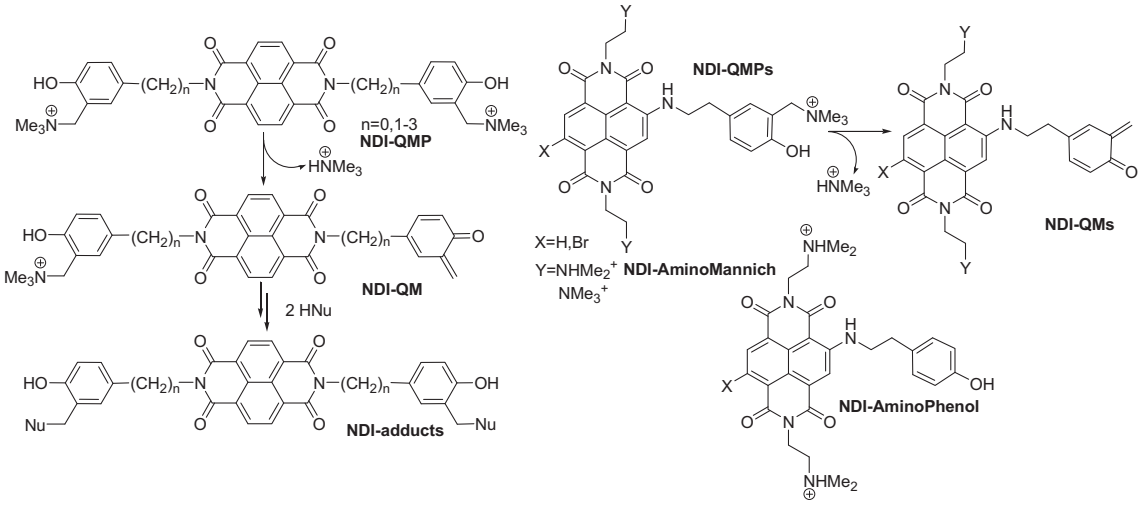

Scheme 1. NDI derivatives conjugated to *ortho*-quinone methide (QM) precursors (QMPs) recently investigated.

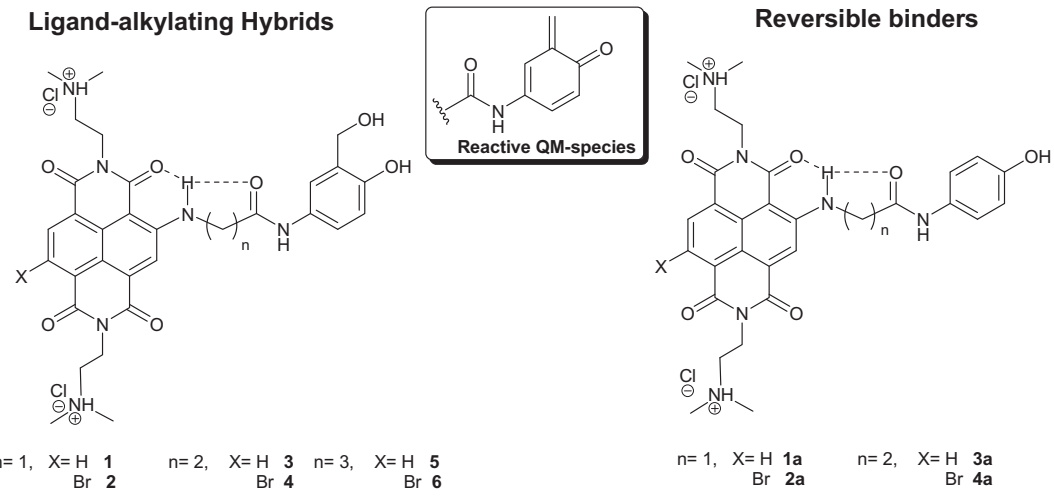

Scheme 2. Tri-substituted NDIs **1**–**6** (as hydrochlorides)exploited as G-4 ligand-alkylating hybrid compounds. The dotted lines highlight the presence of intra-molecular H-bonding which could restrain the conformational mobility of the structures.

A solution of 2-(hydroxymethyl)-4-amino isopropylidenacetal (**13**) (500 mg 1.8 mmol) in 5 ml of DMA was added dropwise to the resulting suspension stirring for 75 min. 20 ml of aqueous $NaHCO_3$ were added to the mixture and after 1 h product **16** was formed as white solid. 65% Yield. ^{1}H NMR (300 MHz, $CDCl_3$, 25 °C, TMS): δ = 7.39 (bs, 1H), 7.14 (bs, 1H), 7.07 (dd, 1H, J = 8.7, 1.9 Hz), 6.78 (d, 1H, J = 8.7 Hz), 4.84 (s, 1H), 3.68 (t, 2H, J = 6 Hz), 2.55 (t, 2H, J = 7 Hz), 2.21 (q, 2H, J = 6.5), 1.54 (s, 6H). ^{13}C NMR (300 MHz, $CDCl_3$): δ = 169.5, 148.0, 130.3, 120.2, 119.7, 117.2, 116.8, 60.8, 44.3, 33.8, 44.3, 33.8, 27.8, 24.6. Anal. Calcd. for $C_{14}H_{18}ClNO_3$: C, 59.26; H, 6.39; Cl, 12.49; N, 4.94; O, 16.92. Found: C, 58.98; H, 6.41; N, 4.96.

The azides **17**–**19** have been prepared following the general procedure of azidation, described in the Supporting information.

2-azido-N-(2,2-dimethyl-4H-benzo[d][1,3]dioxin-6-yl)acetamide (17): 90% yield; white powder. ^{1}H NMR (300 MHz, $CDCl_3$, 25 °C, TMS): δ = 7.9 (s, 1H), 7.30 (d, 1H, J = 2.4 Hz), 7.10 (dd, 1H, J = 2.4 Hz, J = 8.7 Hz), 6.75 (d, 1H, J = 8.7 Hz), 4.9 (s, 2H), 4.10 (s, 2H), 1.50 (s, 6H) ^{13}C NMR (300 MHz, $CDCl_3$): δ = 164.2, 148.4, 129.3, 120.4, 119.7, 117.4, 116.9, 99.6, 60.8, 52.8, 24.6. Anal. Calcd. for $C_{12}H_{14}N_4O_3$: C, 54.96; H, 5.38; N, 7.82; O, 21.36. Found: C, 55.02; H, 5.32; N, 7.88.

3-azido-N-(2,2-dimethyl-4H-benzo[d][1,3]dioxin-6-yl)propanamide (18): 52% yield; brown oil. ^{1}H NMR (300 MHz, $CDCl_3$, 25 °C, TMS): δ = 7.40 (s, 1H), 7.07 (d, 1H, J = 8.6 Hz), 6.79 (d, 1H, J = 8.6 Hz), 4.85 (s, 2H), 3.73 (t, 2H, J = 6.2 Hz), 2.59 (t, 2H, J = 6.2 Hz), 1.55 (s, 6H). Anal. Calcd. for $C_{13}H_{16}N_4O_3$: C, 56.51; H, 5.84; N, 20.28; O, 17.37. Found: C, 56.49; H, 5.80; N, 20.32.

4-azido-N-(2,2-dimethyl-4H-benzo[d][1,3]dioxin-6-yl)butanamide (19): 75% yield; white powder. ^{1}H NMR(300 MHz, $CDCl_3$, 25 °C, TMS): δ = 7.39 (bs, 1H), 7.13 (bs, 1H), 7.07 (dd, 1H, J = 6.6, 2 Hz), 6.79 (d, 1H, J = 8.7 Hz), 4.84 (s, 2H), 3.44 (t, 2H, J = 6.4 Hz), 2.46 (t, 2H, J = 7.1 Hz), 2.03 (q, 2H, J = 6.7 Hz), 1.55 (s, 6H). ^{13}C NMR (300 MHz, $CDCl_3$): δ = 169.7, 148.0, 130.3, 120.2, 119.7, 117.2, 116.8, 99.5, 60.8, 50.6, 33.8, 29.6, 24.6. Anal. Calcd. for $C_{14}H_{18}N_4O_3$: C, 57.92; H, 6.25; N, 19.30; O, 16.53. Found: C, 57.97; H, 6.19; N, 19.32.

The amines **8**–**10** have been synthesized by reduction of the azido derivatives (**17**–**19**), according to the reduction protocol described in the Supporting information.

2-amino-N-(2,2-dimethyl-4H-benzo[d][1,3]dioxin-6-yl)acetamide (8): Yield 80%, yellow oil. ^{1}H NMR (300 MHz, $CDCl_3$, 25 °C, TMS): δ = 8.25 (s, 1H), 7.35 (d, 1H J = 2.50 Hz), 7.10 (d, 1H J = 8.7 Hz), 6.80 (dd, 1H J = 2.4 Hz, J = 8.7 Hz), 4.81 (s, 2H), 4.15 (s, 2H), 3.75 (broad s, 2H), 1.52 (s, 6H). ^{13}C NMR (300 MHz, $CDCl_3$): δ = 164.2, 148.4, 129.3, 120.4, 119.7, 117.4, 116.9, 99.6, 60.8, 52.8, 24.6. Anal. Calcd. for $C_{12}H_{16}N_2O_3$: C, 61.00; H, 6.83; N, 11.86; O, 20.32. Found: C, 61.09; H, 6.88; N, 11.88.

3-amino-N-(2,2-dimethyl-4H-benzo[d] [1,3]dioxin-6-yl)propanamide (9): Yield 71%, yellow oil. ^{1}H NMR (300 MHz, CD_3OD): δ = 7.32 (d, 1H, J = 2.3 Hz), 7.25 (dd, 1H, J = 8.7, 2.5 Hz), 6.74 (d, 1H, J = 8.7 Hz), 3.32 (s, 2H), 3.03 (t, 2H, J = 6.5 Hz), 2.57 (t, 2H, J = 6.5 Hz), 1.51 (s, 6H). ^{13}C NMR (MeOD): δ = 172.5, 149.5, 132.9, 122.1, 121.2, 118.4, 118.3, 101.0, 62.1, 45.0, 39.1, 31.2, 25.2. Anal. Calcd. for $C_{13}H_{18}N_2O_3$: C, 62.38; H, 7.25; N, 11.19; O, 19.18. Found: C, 62.44; H, 7.21; N, 11.23.

4-amino-N-(2,2-dimethyl-4H-benzo[d][1,3]dioxin-6-yl)butanamide (10): Yield 92%, yellow oil. ^{1}H NMR(300 MHz, $CDCl_3$, 25 °C, TMS): δ = 8.89 (s, 1H), 7.37 (bs, 1H), 7.10 (d, 1H, J = 8.6 Hz), 6.71 (d, 1H, J = 8.6 Hz), 4.76 (s, 2H), 2.79 (bs, 2H), 2.4 (bs, 2H), 1.83 (bs, 2H), 1.5 (s, 6H). Anal. Calcd. for $C_{14}H_{20}N_2O_3$: C, 63.62; H, 7.63; N, 10.60; O, 18.16. Found: C, 63.70; H, 7.41; N, 10.56.

2,6-dibromonaphthalene bisanhydride was synthesized according to standard published procedures [53].

Procedure for the synthesis of 7 and 7a. To a stirred suspension of 2,6-dibromo dianhydride (600 mg, 0.001 mol) in acetic acid (15 ml) N,N-dimethylethylamine (1.6 ml) was added. After stirring for 30 min at 130 °C, the reaction mixture was cooled to r.t. and quenched into ice. The crude orange solid was filtered and purified by column chromatography ($CHCl_3$:MeOH 9:1), yielding **7** (45%), **7a** (26%).

***N,N′-Di-(N,N-dimethylethyl)*-2,6-dibromonaphthalene-1,4,5,8-tetra-carboxylic acid bisimide** (**7**). Yellow-orange solid. ^{1}H NMR (200 MHz, $CDCl_3$, 25 °C, TMS): δ = 9.0 (s, 2H), 4.35 (m, 4H), 2.72 (m, 4H), 2.37 (s, 12H). Anal. Calcd. for $C_{22}H_{22}Br_2N_4O_4$: C, 46.66; H, 3.92; Br, 28.22; N, 9.89; O, 11.30. Found: C, 46.69; H, 3.89; Br, 28.18; N, 9.92.

***N,N′-Di-(N,N-dimethylethyl)*-2-bromonaphthalene-1,4,5,8-tetra-carboxylic acid bisimide** (**7a**). Yellow solid. ^{1}H NMR (200 MHz, $CDCl_3$, 25 °C, TMS): δ = 8.94 (s, 1H), 8.84–8.76 (m, 2H), 4.37 (m, 4H), 2.69 (bs, 4H), 2.36 (s, 12H). Anal. Calcd. for $C_{22}H_{23}BrN_4O_4$: C, 54.22; H, 4.76; Br, 16.40; N, 11.50; O, 13.13. Found: C, 54.26; H, 4.71; Br, 16.41; N, 11.55.

Ligands **1**–**6** and **1a**–**4a** have been prepared according to the general method described as following.

Nucleophilic aromatic substitution reaction. The NDIs mixture resulting from the previous step (**7**, **7a**; 250 mg) was solved into 20 ml of DMF containing the amine (0.6 mmol). The mixture

was stirred at 35 °C for 24 h under argon. The resulting red solution was poured in water (100 ml) and crashing out was observed. The collected solid was washed with water and purified by preparative HPLC (C-18 reverse phase column, CH_3CN:H_2O 0.1% TFA, as eluent). Addition of HCl 1 M solution to each chromatographic portion and solvent evaporation under vacuum afforded the adducts as hydrochlorides.

Ligand 1: Yield 46%. ^{1}H NMR (300 MHz, DMSO): δ = 10.32 (s, 1H), 10.22 (s, 1H), 9.71 (bs, 1H), 9.35 (bs, 1H), 8.57 (d, 1H, J = 7.7 Hz), 8.29 (d, 1H, J = 7.7 Hz), 8.04 (s, 1H), 7.57 (bs, 1H), 7.34 (dd, 1H, J = 1.6, 8.4 Hz), 6.73 (d, 1H, J = 8.4 Hz), 4.57 (s, 2H), 4.41 (m, 4H), 3.48 (m, 4H), 2.94 (s, 6H), 2.92 (s, 6H). ^{13}C NMR (CD_3OD): δ = 165.4, 163.4, 163.0, 151.4, 150.2, 130.7, 130.2, 128.9, 127.7, 126.1, 124.0, 123.0, 120.4, 119.1, 118.8, 118.7, 118.5, 114.4, 99.4, 58.0, 54.6, 45.8, 42.7, 33.0. Anal. Calcd. for $C_{31}H_{36}Cl_2N_6O_7$: C, 55.11; H, 5.37; Cl, 10.50; N, 12.44; O, 16.58. Found: C, 55.14; H, 5.31; Cl, 10.54; N, 12.48.

Ligand 1a: Yield 41%. ^{1}H NMR (300 MHz, CD_3OD): δ = 10.09 (s, 1H), 8.44 (d, 1H, J = 7.8 Hz), 8.19 (d, 1H, J = 7.04 Hz), 7.86 (s, 1H), 7.42 (d, 2H, J = 7.8 Hz), 6.79 (d, 2H, J = 7.8 Hz), 4.53 (bs, 4H), 4.36 (s, 2H), 3.57 (bs, 4H), 3.03 (s, 12H). Anal. Calcd. for $C_{30}H_{34}Cl_2N_6O_6$: C, 55.82; H, 5.31; Cl, 10.98; N, 13.02; O, 14.87. Found: C, 55.86; H, 5.28; Cl, 11.02; N, 13.07.

Ligand 2: Yield 30%. ^{1}H NMR (300 MHz, CD_3OD): δ = 8.65 (s, 1H), 8.11 (s, 1H), 7.57 (d, 1H, J = 2.5 Hz), 7.35 (dd, 1H, J = 2.5, 8.6 Hz), 6.77 (d, 1H, J = 8.6 Hz), 4.66 (s, 2H), 4.58 (bs, 4H), 4.47 (s, 2H), 3.57 (bs, 4H), 3.05 (s, 12H). ^{13}C NMR (CD_3OD): δ = 171.4, 168.2, 164.0, 162.2, 161.8, 153.3, 153.0, 138.9, 134.4, 129.8, 128.9, 127.9, 125.5, 123.1; 122.7, 122.5, 121.9, 116.1, 101.3, 60.9, 57.7, 57.3, 47.2, 44.5, 38.6, 37.0. Anal. Calcd. for $C_{31}H_{35}BrCl_2N_6O_7$: C, 49.35; H, 4.68; Br, 10.59; Cl, 9.40; N, 11.14; O, 14.84. Found: C, 49.39; H, 4.65; Br, 10.58; Cl, 9.37; N, 11.16.

Ligand 2a: Yield 34%. ^{1}H NMR (300 MHz, CD_3OD): δ = 10.09 (s, 1H), 8.56 (s, 1H), 8.13 (s, 1H), 7.42 (d, 2H, J = 7.8 Hz), 6.77 (d, 2H, J = 7.8 Hz), 4.54 (bs, 4H), 4.43 (s, 2H), 3.55 (bs, 4H), 3.02 (s, 12H). Anal. Calcd. for $C_{30}H_{33}BrCl_2N_6O_6$: C, 49.74; H, 4.59; Br, 11.03; Cl, 9.79; N, 11.60; O, 13.25. Found: C, 49.77; H, 4.61; Br, 11.01; Cl, 9.81; N, 11.62.

Ligand 3: Yield 39%. ^{1}H NMR (300 MHz, CD_3OD): δ = 8.29 (d, 1H; J = 7.8 Hz), 8.03 (m, 2H), 7.54 (d, 1H, J = 2.5 Hz), 7.26 (dd, 1H, J = 2.5, 8.6 Hz), 6.72 (d, 1H, J = 8.6 Hz), 4.62 (s, 2H), 4.50 (m, 4H), 3.94 (bs, 2H), 3.55 (m, 4H), 3.05 (s, 6H), 2.99 (s, 6H), 2.88 (m, 2H). ^{13}C NMR (CD_3OD): δ = 171.6, 167.2, 164.9, 164.7, 164.5, 153.4, 153.3, 132.4, 131.8, 130.7, 129.4, 128.9, 127.1, 125.6, 124.2, 122.5, 122.4, 121.2, 120.4, 116.2, 100.5, 60.9, 57.5, 57.1, 44.5, 44.4, 40.9, 37.2, 36.9. Anal. Calcd. for $C_{32}H_{38}Cl_2N_6O_7$: C, 55.74; H, 5.55; Cl, 10.28; N, 12.19; O, 16.24. Found: C, 55.71; H, 5.52; Cl, 10.32; N, 12.14.

Ligand 3a: Yield 52%. ^{1}H NMR (300 MHz, CD_3OD): δ = 9.91 (s, 1H), 8.34 (d, 1H, J = 7.8 Hz), 8.07 (d, 1H, J = 7.8 Hz), 8.06 (s, 1H), 7.38 (d, 2H, J = 8.8 Hz), 6.75 (d, 2H, J = 8.8 Hz), 4.52 (m, 4H), 3.96 (t, 2H, J = 5.7 Hz), 3.56 (m, 4H), 3.49 (t, 2H, J = 5.7 Hz), 3.04 (s, 12H). ^{13}C NMR (CD_3OD): δ = 169.8, 165.4, 163.2, 162.9, 154.0, 151.6, 130.6, 130.0, 128.9, 127.2, 125.4, 123.8, 122.4, 121.9, 119.4, 118.7, 114.7, 98.7, 55.7, 55.4, 42.6, 42.5, 39.0, 35.3, 35.0. Anal. Calcd. for $C_{31}H_{36}Cl_2N_6O_6$: C, 56.45; H, 5.50; Cl, 10.75; N, 12.74; O, 14.55. Found: C, 56.48; H, 5.47; Cl, 10.72; N, 12.71.

Ligand 4: Yield 27%. ^{1}H NMR (300 MHz, CD_3OD): δ = 8.42 (s, 1H), 8.18 (s, 1H), 7.54 (d, 1H, J = 2.3 Hz), 7.28 (dd, 1H, J = 2.3, 8.6 Hz), 6.73 (d, 1H, J = 8.6 Hz), 4.76 (s, 2H), 4.52 (m, 4H), 3.97 (bs, 2H), 3.51 (m, 4H), 3.05 (s, 6H), 2.97 (s, 6H), 2.91 (m, 2H). ^{13}C NMR (CD_3OD): δ = 171.6, 167.0, 163.7, 163.6, 162.9, 153.3, 153.0, 138.8, 131.8, 129.8, 129.5, 128.5, 124.2, 122.6; 122.4, 122.0, 121.3, 116.1, 100.7, 60.9, 57.4, 57.1, 44.4, 40.9, 37.7, 37.1, 37.0. Anal. Calcd. for $C_{32}H_{37}BrCl_2N_6O_7$: C, 50.01; H, 4.85; Br, 10.40; Cl, 9.23; N, 10.94; O, 14.57. Found: C, 50.05; H, 4.88; Br, 10.39; Cl, 9.18; N, 10.97.

Ligand 4a: Yield 25%. ^{1}H NMR (300 MHz, CD_3OD): δ = 8.53 (s, 1H), 8.26 (s, 1H), 7.38 (d, 2H, J = 8.9 Hz), 6.75 (d, 2H, J = 8.9 Hz), 4.54 (m, 4H), 4.01 (m, 2H), 3.54 (m, 4H), 3.47 (m, 2H), 3.05 (s, 6H), 2.98 (s, 6H). ^{13}C NMR (CD_3OD): δ = 167.2, 163.8, 163.7, 163.0, 155.9, 153.1, 138.9, 131.8, 130.0, 128.7, 124.6, 124.4, 123.8, 122.9, 122.0, 121.3, 116.6, 100.8, 57.5, 57.2, 44.4, 40.8, 37.6, 37.1, 37.0. Anal. Calcd. for $C_{31}H_{35}BrCl_2N_6O_6$: C, 50.42; H, 4.78; Br, 10.82; Cl, 9.60; N, 11.38; O, 13.00. Found: C, 50.43; H, 4.75; Br, 10.79; Cl, 9.63; N, 11.41.

Ligand 5: Yield 36%. ^{1}H NMR(300 MHz, CD_3OD): δ = 8.41 (d, 1H, J = 7.7 Hz), 8.15 (d, 1H, J = 7.8 Hz), 8.11 (s, 1H), 7.37 (d, 1H, J = 2 Hz), 7.17 (dd, 1H, J = 8.5, 2.2 Hz), 6.61 (d, 1H, J = 8.6 Hz), 4.55 (bs, 4H), 4.47 (bs, 2H), 3.74 (bs, 2H), 3.56 (bs, 2H), 3.49 (bs, 2H), 3.03 (s, 12H), 2.57 (t, 2H, J = 6.1 Hz), 2.21 (t, 2H, J = 6.2 Hz). ^{13}C NMR (CD_3OD): δ = 173.2, 167.3, 165.1, 164.8, 164.7, 153.9, 153.0, 132.3, 132.0, 130.9, 129.2, 129.1, 127.4, 125.6, 124.4, 122.0, 121.8, 121.4, 120.7, 115.9, 100.7, 61.0, 57.6, 57.3, 44.4, 44.4, 44.1, 43.9, 37.2, 36.7, 35.1, 26.6. Anal. Calcd. for $C_{33}H_{40}Cl_2N_6O_7$:C, 56.33; H, 5.73; Cl, 10.08; N, 11.94; O, 15.92. Found: C, 56.35; H, 5.69; Cl, 10.05; N, 11.96.

Ligand 6: Yield 22%, ^{1}H NMR(300 MHz, CD_3OD): δ = 8.59 (s, 1H), 8.26 (s, 1H), 7.30 (bs, 1H), 7.15 (dd, 1H, J = 8.5, 2.3 Hz), 6.57 (d, 1H, J = 8.5 Hz), 4.55 (bs, 4H), 4.47 (bs, 2H), 3.78 (t, 2H, J = 5.9 Hz), 3.56 (bs, 2H), 3.49 (bs, 2H), 3.04 (s, 12H), 2.56 (t, 2H, J = 6.2 Hz), 2.22 (t, 2H, J = 6.2 Hz). ^{13}C NMR (CD_3OD): δ = 173.2, 167.2, 162.0, 163.8, 163.2, 153.5, 153.0, 138.9, 132.0, 130.2, 129.2, 128.7, 124.7, 124.5, 123.0, 122.2, 121.7, 121.6, 121.2, 115.8, 101.0, 60.9, 57.5, 57.3, 50.1, 49.9, 49.6, 49.3, 49.0, 48.7, 48.4, 44.5, 44.0, 37.6, 36.9, 35.2, 26.6. Anal. Calcd. for $C_{33}H_{39}BrCl_2N_6O_7$:C, 50.65; H, 5.02; Br, 10.21; Cl, 9.06; N, 10.74; O, 14.31. Found: C, 50.64; H, 5.06; Br, 10.18; Cl, 9.01; N, 10.78.

2.2. Computation

A preliminary conformational search was carried out at the semi-empiric level using PM3 level of theory. The search was performed with the Spartan stochastic Monte Carlo search algorithm that is implemented in the software package. This search resulted in more than 20 minima. All the conformational structures resulting from this search provided initial geometries for the electronic structure calculations. Geometries of all conformers were optimized at the density functional theory (DFT) level with the Gaussian 03, Revision C.02 software package [54]. These calculations were performed using gradient corrected DFT with the Becke-Lee-Young-Parr composite exchange correlation functional (B3LYP) [55] as implemented in the Gaussian suite of programs for electronic structure calculations. Single-point energy calculations in aqueous solvent on the optimized gas phase geometries were performed for all the conformers by PCM solvation model, using UAHF atomic radii [56]. For the most stable conformers (**NDI-Mod3a** and **NDI-Mod3b**), geometry optimization was performed using a more extended basis set including a double-ζ basis set augmented by diffuse s functions on C, N, and O and polarized d functions on C, N, and O and p function on H [6-31 + G(d,p)]. Full geometry optimization in gas phase at PCM-B3LYP/6-31G(d) level was performed for the conformers **NDI-Mod3a** and **NDI-Mod3b**. Finally, single-point energies on the B3LYP/6-31 + G(d,p) gas phase geometries were computed to evaluate solvation effect at PCM-B3LYP/6-31 + G(d,p) level of theory.

2.3. FRET-melting assay

All oligonucleotides were purchased from Sigma–Aldrich. After an initial dilution at 1 mM in purified water, further dilutions were carried out in the relevant buffer. FRET assay was performed with F21T (5′-d(*FAM*-$G_3[T_2AG_3]_3$-*Tamra*-3′) with *FAM*: 6-carboxyfluorescein and *Tamra*: 6-carboxy-tetramethylrhodamine). Fluorescence melting curves were determined with a LightCycler II (Roche) real-time PCR machine, using a total reaction volume of 20 μL, with 0.25 μM of

tagged oligonucleotide in a buffer containing 10 mM lithium cacodylate pH 7.4 and 50 mM KCl. After a first equilibration step at 30 °C during 2 min, a stepwise increase of 1 °C every minute for 65 cycles to reach 95 °C was performed and measurements were made after each cycle with excitation at 470 nm and detection at 530 nm. The melting of the G-quadruplex was monitored alone or in the presence of various concentrations of compounds and/or of G4 competitor 27NHEG (5′-d(TGGGGAGGGTGGGGAGGGTGGGGAAGG)-3′), double-stranded competitor ds26 (5′-d(CAATCGGATCGAATTCGATCCGATTG)-3′) and single-stranded 4GGG scrambled (5′-d(GGATGTGAGTGTGAGTGTGAGG)-3′). Final analysis of the data was carried out using Excel and Sigma Plot software. Emission of FAM was normalized between 0 and 1, and $T_{1/2}$ was defined as the temperature for which the normalized emission is 0.5. $\Delta T_{1/2}$ values are mean of 2–3 experiments ± standard deviation.

2.4. CD analysis

CD experiments were performed on a Jasco J 810 spectropolarimeter equipped with a NESLAB temperature controller and interfaced to a PC100. A quartz cuvette with 5 mm path length was used for spectra recorded from 230 to 320 nm at 2 nm bandwidth, 0.1 nm step size, and 4 s time per point. The reported spectrum of each sample represents the average of 2 scans. Observed ellipticities were converted to mean residue ellipticity $(\theta) = \text{deg} \times \text{cm}^2 \times \text{dmol}^{-1}$ (Molar Ellipticity). The oligomer 4GGG (5′-d(AGGG[TTAGGG]$_3$)-3′) was diluted from stock to the final concentration (4 μM) in lithium cacodylate buffer (10 mM, pH 7.4) with 50 mM KCl and then annealed by heating at 95 °C for 5 min, gradually cooled to room temperature, and measured after 24 h. Compounds at 16 μM final concentration were added after 4GGG annealing. CD titrations were performed at a fixed 4GGG concentration (usually 3–4 μM) with various concentrations (0–16 mol equiv) of ligands at 20 °C. All samples were allowed to equilibrate overnight. A buffer baseline was collected in the same cuvette and subtracted from the sample spectra.

Analysis of the binding data was carried out using Excel and Sigma Plot software.

For the thermal unfolding experiments, CD spectra were recorded from 20 °C to 95 °C, with temperature increase of 5 °C, and processed as above. T_m and ΔH values were calculated according to the van't Hoff equation, applied for a two state transition from a folded to unfolded state, assuming that the heat capacity of the folded and unfolded states are equal [57].

2.5. Surface plasmon resonance study (SPR)

SPR measurements were performed with BIAcore T100 (GE Healthcare) system using streptavidin-coated sensor chips (Series S Sensor chip SA, GE Healthcare). The 5′- biotinylated sequence (4GGG DNA) were heated to 95 °C and annealed by slow cooling to form quadruplex in filtered and degassed 10 mM HEPES buffer with 200 mM KCl with 0.005% surfactant Tween 20, at pH 7.4. Flow cell 2 was used as sample flow cell for the immobilization of the biotinylated oligo. Flow cells 1 was left blank as control to account for any signal generated owing to bulk solvent effect or any other effect not specific to the DNA interaction, which was subtracted from the signal obtained in flow cell 2. All experiments were performed at 25 °C using running buffer (0.22 μm filtered and degassed 10 mM HEPES with 200 mM KCl and 0.005% surfactant Tween 20) at pH 7.4. Oligonucleotide immobilized surface was exposed to the running buffer for at least 2 h at a flow rate of 30 μl min^{-1} for attaining baseline stability. **1** and **1a** analyte solutions at different concentrations (1×10^{-9} M to 1×10^{-6} M) were prepared in the running buffer and were injected (at 30 μl min^{-1} for 120 s) in series. Following this, dissociation from the surface was monitored for 300 s in running buffer. Regeneration was done using 10 mM glycine. Analysis of the binding sensorgrams was carried out using 1:1 binding sites model using BIA evaluation software 2.0.3. The experiments were carried out in triplicates and the standard error was calculated.

2.6. Alkylation

For the oligonucleotide alkylation experiment, the gel-purified and desalted 4GGG, or 4GGG scrambled (5′-d(GGATGTGAGTGTGAGTGTGAGG)-3′) oligonucleotides were 5′-end-labelled with [γ-^{32}P]ATP by T4 polynucleotide kinase and purified by MicroSpin G-25 columns (Amersham Biosciences, Europe). After purification, the oligonucleotides were re-suspended in G4 buffer (lithium cacodylate 10 mM, pH 7.4, KCl 50 mM), heat-denatured and folded. Before heat-denaturation 4GGG scrambled DNA was alternatively incubated with its complementary strand to obtain the ds oligonucleotide. Compounds **1**, **2**, **3**, **4**, **5** and **6** reactions with the labelled oligonucleotide (5 pmol/sample) were performed at 40 °C in G4 buffer. These conditions were selected to maintain the stability of the target oligonucleotide structures and to obtain thermal activation of the compounds. After 24 h, samples were ethanol-precipitated, re-suspended in formamide gel-loading buffer, and heated at 95 °C for 4 min. Reaction products were analyzed on 20% denaturing polyacrylamide gels and visualized by phosphorimaging analysis (Molecular Dynamics, Amersham Biosciences). Quantification was performed by ImageQuant software (Molecular Dynamics).

The alkylation band was excised from the gel and the product eluted in mQ water, purified by MicroSpin G-25 columns, and digested with 0.5 units of Exonuclease I (Fermentas) in supplied buffer (67 mM glycine–KOH, 6.7 mM $MgCl_2$, 1 mM DTT) for 30 min at 37 °C. Digestion was stopped by ethanol-precipitation and samples were run on 20% denaturing polyacrylamide gels and visualized by phosphorimaging analysis (Molecular Dynamics, Amersham Biosciences).

2.7. Cytotoxicity

Telomerase-positive human cells were: lung carcinoma cells A549 (ATCC number CCL-185) and human colorectal adenocarcinoma cells HT-29 (ATCC number HTB-38). Telomerase-negative human cells were human foreskin fibroblast HFF-1 (ATCC number SCRC-1041). Cell lines were obtained from American Type Culture Collection (Rockville, MD). Cells were maintained as a monolayer in the logarithmic growth phase at 37 °C in a 5% CO_2 humidified atmosphere, using Dulbecco's modified Eagle's medium supplemented with 10% foetal calf serum and penicillin (100 units/mL)/streptomycin (100 μg/mL) (A549 and HT-29). Cytotoxic effects on tumour cell growth were determined by MTT assay. NDIs were dissolved and diluted into working concentrations with DMSO. Cells (1.75×10^4 cells/well) were plated onto 96-microwell plates to a final volume of 100 μL and allowed an overnight period for attachment. At day 1, 1 μL of each dilution of tested compounds was added per well to get a 1% final concentration of drug solvent per well. Control cells (without any compound but with 1% drug solvent) were treated in the exact same conditions. Cell survival was evaluated by an MTT assay: 10 μL of freshly dissolved solution of MTT (5 mg/mL in PBS) were added to each well, and after 4 h of incubation, 100 μL of solubilization solution [10% sodium dodecyl sulphate (SDS) and 0.01 M HCl] were added. After overnight incubation at 37 °C, absorbance was read at 540 nm. Data were expressed as mean values of three individual experiments conducted in triplicate.

The percentage of cell survival was calculated as follows: cell survival = (*A*well−*A*blank)/(*A*control−*A*blank) × 100, where blank denotes the medium without cells.

3. Results and discussion

3.1. Structural features of the ligand-alkylating hybrid compounds

The ligands (**1**–**6**) in Scheme 2 exhibit common structural features, such as two $-(CH_2)_2NMe_2$ solubilizing side chains tethered to both the imides and an additional phenol moiety, which has been linked to the NDI aromatic core by modular alkyl-amido spacers. The first structural diversity is the length of the spacer and its conformational mobility, improved by adding methylene units (from $n = 1$ to $n = 3$, Scheme 2). The second key structural difference is the *orto*-CH_2OH group on the phenol moiety. Its presence confers alkylating properties to the NDIs **1**–**6**, through a mild QM generation. Therefore, on the basis of the Y substituent (Scheme 3), it has been possible to define two distinctive subclasses among the NDIs listed: (i) potential reversible G-4 binders (**1a**–**4a**; Y=H, Scheme 3) and (ii) hybrid ligand-alkylating NDIs (**1**–**6**, Y=CH_2OH). The key step of the synthetic protocol is the mild nucleophilic aromatic substitution (S_NAr) on both the NDIs **7** and **7a** with the amines **8**–**12** (step c, Scheme 3).

3.2. Synthesis of the QMPs units

The QMP intermediates **8**–**10** and the phenol unreactive analogues **11**, **12** (Scheme 3) to be tethered to the NDI scaffold have been prepared according a general synthetic procedure depicted in Scheme 4 (Supporting information). The synthesis started from the 2-(hydroxymethyl)-4-aminophenylpropyliden acetal (**13**) prepared according to standard procedures. The first step was a nucleophilic acyl substitution on the chloroacyl chloride by the aniline **13**. Three different acyl chlorides (chloroacetyl chloride, 3-chloropropionyl chloride, 4-chlorobutyryl chloride) have been used to modulate the length of the tethering chain. The reaction with chloroacetyl chloride (i, Scheme 4) was almost quantitative, unlike those using 3-chloropropionyl (ii) and 4-chlorobutyryl chloride (iii), where reaction yields have been affected by the competing elimination reaction. The final steps of this synthetic route were: (iv) nucleophilic substitution with sodium azide in DMF and (v) reduction of

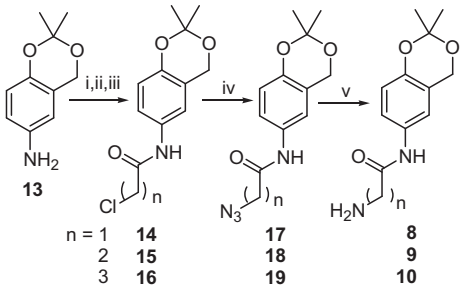

Scheme4. Synthesis of the **QMP** units to be tethered to the NDI core. (i) Chloroacetyl chloride THF, TEA, 2 h, 0 °C; (ii) 3-Chloropropionyl chloride,CH_3CN, $NaHCO_3$, 2 h, r.t.; (iii) 4-Chlorobutyryl chloride, DMA, $NaHCO_3$, 2 h, r.t.; (iv) NaN_3, DMF, 10 h, 80 °C; (v) $NaBH_4$, NaOH, Pd/C 10%, THF dry, 30 min, r.t.

the resulting azides (**17**–**19**) to afford the amines **8**–**10** in good yields, which have been used in the final S_NAr step. The amines **11** and **12** have been prepared following an identical synthetic protocol starting from 4-aminophenol (see Supporting information).

3.3. Conjugation of the QMPs to the NDI core

Recently, microwaved assisted functionalization of both 2,6-dichloro- and 2,6-dibromo-NDIs (**7**) by aromatic nucleophilic substitution (S_NAr) has been achieved with low yields (11–19%), using commercial amines as solvent and high temperature ($T = 150$ °C) [36]. Such a protocol could not be exploited for tethering the amine **8**–**10** to the NDI core. In fact, under the harsh conditions required by the published protocol, the QMP moieties of the NDIs underwent fast degradation through QM generation, resulting in a sloppy mixture of oligomers. In addition, the above conditions are not only inefficient, but also unnecessary. In fact, the synthesis of the final QMP-NDI conjugated structures (**1**–**6**, Scheme 3) were carried out starting from a mixture of 2-bromo- and 2,6-dibromo-NDI (**7a** and **7**, respectively) with the amines **8**–**12,** in a stoichiometric ratio, by a mild and efficient S_NAr. The NDIs **7** and **7a** have been synthesized in mixture according to an optimized two-steps synthesis, starting from the commercially available 1,4,5,8-naphthalene-tetra-carboxylic dianhydride. The

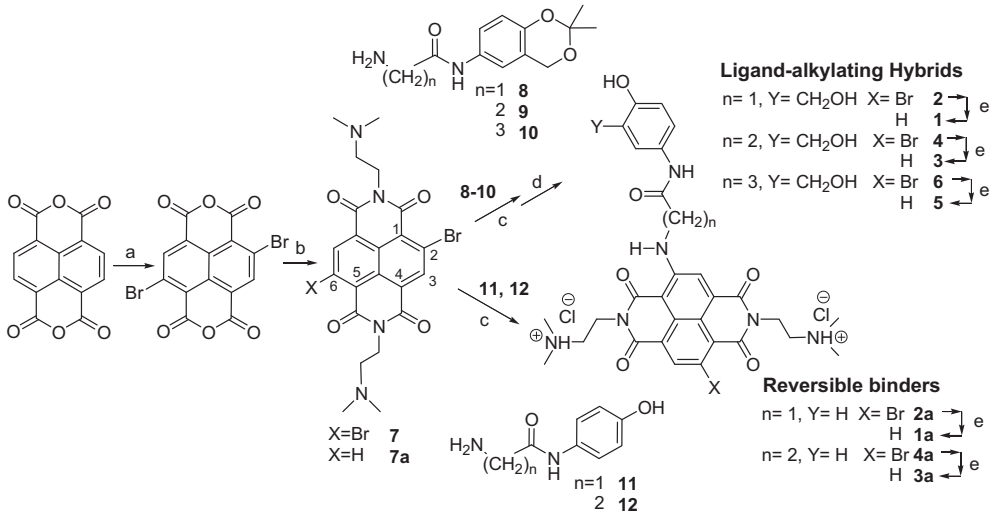

Scheme 3. Synthesis of the tri-substituted NDIs **1**–**6**.Reagent and conditions: (a) dibromoisocyanuric acid (DBI), H_2SO_4, reflux, 12 h, yield 93%; (b) dimethylethylamine, acetic acid, 130 °C, 30 min. (c) Amine **8**–**12**, DMF, 35 °C, 24 h d) Deprotection, THF:H_2O 1:1, 0.5% HCl e) Reductive debromination, $Na_2S_2O_4$, in water, 2 h.

first step (a, Scheme 3) is a selective 2,6-dibromination of the anhydride with dibromocyanuric acid (DBI) in concentrated H_2SO_4, followed by (b) an imidation procedure using N,N-dimethylethylendiamine, yielding **7** (45%), and **7a** (26%) in mixture. **7a** was the result of a competing reductive debromination process. The key step for the conjugation of the QMP to the NDI aromatic core is the S_NAr reaction (c, Scheme 3), which has been performed on the **7**–**7a** mixture resulting from the imidization step, without any further purification. The S_NAr selectively generated the asymmetrically disubstituted NDIs **2**, **2a**, **4, 4a** and **6** (bearing both a bromine and an alkylamino moiety on the NDI aromatic ring), together with the monosubstituted NDIs **1**, **1a**, **3, 3a** and **5** (Scheme 3). The resulting substituted NDIs protected as isopropyledene acetals were used without further purification in the last deprotection step (d, Scheme 3). The final NDIs **1**–**6** have been isolated and purified by preparative HPLC (using acetonitrile:water with CF_3COOH 0.1%). The trifluoacetate anion has been exchanged with chloride anion for a better spectroscopic characterization. In order to maximise the efficiency of the synthesis yielding the NDIs **1**, **1a**, **3**, **3a** and **5**, the conversion of the Br-substituted NDIs **2**, **2a**, **4, 4a** and **6** have been achieved by reductive debromination using $Na_2S_2O_4$ (e, Scheme 3), according to a published synthetic protocol [53].

3.4. Modelling the conformational mobility of the alkyl amido side chains

The choice of the alkyl-amido spacers connecting the NDI core to the QMP has been suggested by the following aspects: (i) the replacement of the quaternary ammonium as good leaving group with an uncharged one, such as the hydroxyl group, requires an electron rich phenol aromatic ring (by the amido group) to generate the alkylating QM under very mild conditions [45]; (ii) the alkyl-amido spacers may reduce the conformational mobility of the reactive moiety through an H-bonding network (dotted lines in Scheme 2), extending the flat shape of the NDI core. In addition, the length of the spacer should also affect the lipophilicity of the resulting NDIs. In order to evaluate the conformational mobility, we compared two simplified tri-substituted NDI models **NDI-Mod1**, and **NDI-Mod2** (Scheme 5) exhibiting single and double methylene spacers, respectively, by DFT calculation at B3LYP/6-31G(d) level of theory. A more refined model **NDI-Mod3** has further been investigated at B3LYP/6-31 + G(d,p) level of theory in both gas phase and water bulk, using polarizable continuum models (PCMs).

The conformational potential energy surfaces (PES) of both **NDI-Mod1** and **NDI-Mod2** have been preliminary explored by a PM3 semi-empirical method using the Monte Carlo stochastic approach. This search yielded a single minimum for the **NDI-Mod1** and more several minima for the flexible **NDI-Mod2.** The structures from this search provided initial geometries for the electronic structure calculations. Geometries of all conformers were optimized at the density functional theory (DFT) level with the Gaussian 03 package. These calculations were performed with the 6-31G(d) basis, in the gas phase. **NDI-Mod1** exists as a single conformer (**NDI-Mod1a**, Fig. 1) characterized by two strong intra-molecular H-bonding, which freeze the structures of the spacer coplanar to the NDI aromatic core. On the contrary, 5 different minima, with very similar energy in gas phase (**NDI-Mod2a**–**e**, Fig. 1), have been located for the NDI with a longer spacer (**NDI-Mod2**). Solvent effect computed by single-point calculation on the gas phase geometries at B3LYP/6-31G(d) by PCM solvation model, did not dramatically affect their relative energies (Fig. 1, data in parenthesis). Among them, only **NDI-Mod2c** exhibits a structure with the spacer planar to the NDI core.

The conformational model **NDI-Mod1** was further implemented to the **NDI-Mod3** (Scheme 5) in order to investigate the effect of the phenol moiety on the molecular shape of the tri-substituted **NDIs 1**, **2**, **1a** and **2a** at higher level of theory [B3LYP/6-31 + G(d,p)]. Two different conformations have been located **NDI-Mod3a** and **NDI-Mod3b** (Fig. 2). The former, which is the most stable both in gas phase and in water solution, is completely planar. The relative stability of the planar conformer **NDI-Mod3a** is remarkable in aqueous solution where it lays more than 5 kcal/mol below the non-planar **NDI-Mod3b** (Table 1).

These data suggest that the NDIs **1**, **2**, **1a** and **2a**, with the shortest alkyl-amido spacer ($n = 1$), exhibit planar and fairly rigid shape, unlike the NDIs **3**–**6** and the **NDI-AminoPhenol** (Scheme 1), which benefit of a much higher degree of freedom, due to a longer ($n = 2$, 3) and conformational more flexible spacers. Such a conformational difference should be taken into account to rationalise any striking difference in the biophysical properties between these NDIs.

3.5. Non-alkylating NDI derivatives selectively bind human telomeric G-quadruplex folded DNA

The NDIs conjugated to the phenol moiety by alkyl-amido spacers with increasing chain length were tested ($n = 1$, 2 and 3 for compounds **1**, **3** and **5**, respectively, Scheme 2). The presence of a Br atom on the NDI core centrosymmetric to the side chain was also evaluated on compounds **2**, **4** and **6** (Scheme 2). These compounds are all NDI-QMP conjugates and could hence be triggered by mild thermal activation [43]. In addition, compounds that lack the *ortho*-hydroxymethyl moiety on the side chain phenol were included as reversible non-alkylating ligands (NDIs **1a**, **2a**, **3a** and **4a**, Scheme 3), in order to be able to discriminate the effect of reversible and covalent binding towards the nucleic acids.

The ability of the non-alkylating NDI scaffolds to selectively bind the G-quadruplex (G-4) conformation of the F21T telomere-like DNA oligonucleotide was tested by FRET-melting analysis. The alkylating NDIs were not included because digestion at temperature higher than 40 °C would have triggered QM generation.

Results are reported as the increase in the melting temperature ($\Delta T_{1/2}$) of F21T in K^+ solution caused by the treatment with 1.0 μM

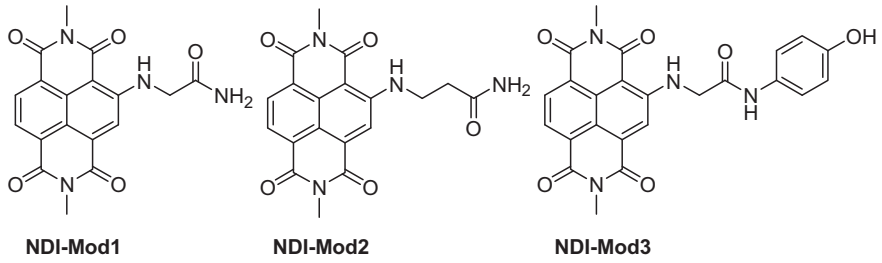

Scheme 5. Simplified tri-substituted NDI models (**NDI-Mod1**-**3**) used to evaluate the conformational mobility of the tethering alkyl-amido spacers.

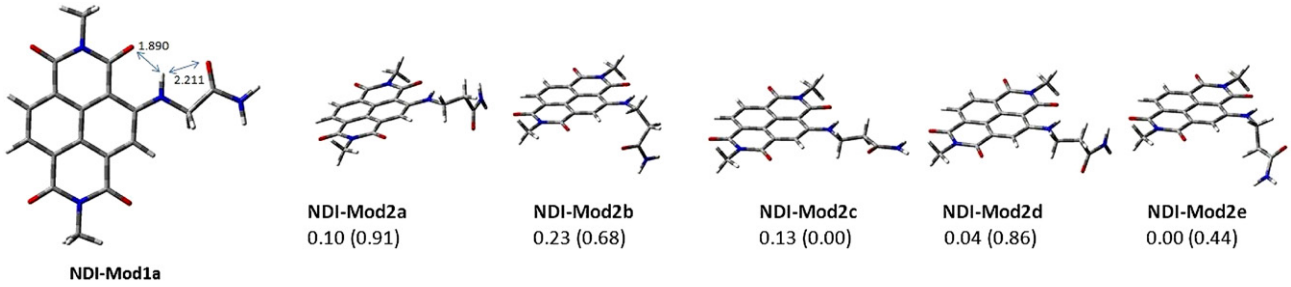

Fig. 1. Computed geometries in the gas phase [at B3LYP/6-31G(d) level] for the conformers NDI-Mod1a and NDI-Mod2a–e. For the latter, relative energies (in kcal/mol) in the gas phase and in aqueous solvent (in parenthesis, by PCM single-point calculation) are reported.

NDIs (Table 2). Derivative **1a** had the most important effect on telomeric G-4 stabilization, with a $\Delta T_{1/2}$ value of 20.9 °C, which is lower than $\Delta T_{1/2}$ values reported for other NDI compounds (10.5 °C $\leq \Delta T_{1/2} \leq$ 35.2 °C at 0.5 μM) [36,39]. In general, compounds with $n = 1$ (**1a** and **2a**) were better stabilizers than those with $n = 2$ (**3a** and **4a**) and H-derivatives (**1a** and **3a**) displayed improved stabilization over the Br-derivatives (**2a** and **4a**) (Table 2). In addition **1a** performed better than **NDI-amino-Mannich** (Scheme 1), a tri-substituted alkylamino NDI recently investigated by us [52], indicating that the introduction of an alkyl-amido spacer in the NDI side chain improves G-4 recognition.

Next, G-4 selectivity for **1a** and **2a** compounds was assessed by FRET-based competition assay, where the ability of the NDI to retain G-4 stabilizing affinity was challenged by non-fluorescent duplex (ds26), single-stranded (scrambled G-4), or G-4 forming DNA (27NHEG) [58]. The latter was the only DNA capable of effectively competing with the labelled sequence: at 27NHEG:F21T molar ratio of 1, $\Delta T_{1/2}$ decreased by 65% and 68% for **1a** and **2a**, respectively, at molar ratio of 10 the drop was almost complete (95% and 94% for **1a** and **2a**, respectively). In contrast, dsDNA was not able to compete so efficiently: at a molar ratio of 1, $\Delta T_{1/2}$ decrease was 15% and 7% for **1a** and **2a**, respectively; at molar ratio of 10, $\Delta T_{1/2}$ decreased by 60% and 55% for **1a** and **2a**, respectively (Table 2). Hence, at molar ratio of 10, G-4 DNA competed 7–8 times better than dsDNA. Finally, ssDNA did not compete at all, even at molar ratio of 10. These results show that the present NDI derivatives, can be considered a fairly promising and selective G-4 binding ligands.

The best performing compound, **1a**, was incubated with 4GGG DNA, a non-labelled oligonucleotide exhibiting four repeats of the human telomeric DNA sequence, and analyzed by CD to check the preferred stabilized G-4 conformation. To ensure equilibrium, samples were left to equilibrate 24 h before CD spectra measurement. In these conditions the 4GGG oligonucleotide presented a major positive peak at 290 nm and a shoulder at 265 nm, which indicated a mixed antiparallel/parallel G-4 form [59]. A minor positive peak at 250 nm is also present, probably indicating a small amount of unfolded DNA [60]. Upon incubation with **1a**, the positive peak a 290 nm increased and those at 265 and 250 nm decreased, indicating a binding event that induced stabilization of the antiparallel G-4 conformation over the parallel one (Fig. 3A). The stability of 4GGG DNA in the presence of the compound was analyzed by CD thermal unfolding and compared to that of 4GGG DNA alone (Fig. 3B and Fig. 1S Supplementary Information). The CD spectra of **1a** incubated with the folded 4GGG DNA were recorded at increasing temperature (range 20–95 °C). At 20 °C the spectrum showed a positive peak at 290 nm, which remained stable up to 50 °C. At 55 °C the peak at 290 nm started to decrease and a positive peak at 265 nm appeared. This latter reached its maximum at 65 °C, after which temperature it began to decrease. At 95 °C no evident peak was present indicating the completeness of DNA unfolding. T_m, separately calculated for the denaturation at 290 nm and 265 nm by the van't Hoff equation, was 64 °C and 80 °C, respectively (Fig. 3B). 4GGG in the absence of the NDI showed one major CD peak at 290 nm, which remained stable up to 50 °C and then decreased rapidly up to 75 °C, temperature at which no more peaks were present. The shoulder at 265 nm slightly decreased over temperature. In these conditions 4GGG exhibited a T_m value of 61 °C (Fig. 3B). This experiment shows that **1a** stabilizes the mixed parallel–antiparallel topology of G-4 telomeric DNA at temperature below 50 °C. However, ligand stabilization of the above conformation is minor (ΔT_m 3 °C). At temperature above 50 °C, the prevalent G-4 topology is parallel-like and this conformation is effectively stabilized by the interaction with the NDI (ΔT_m 19 °C). This latter ΔT_m value is in line with the FRET-melting data (20 °C). The apparent ΔH difference between the unfolding of the G-4 DNA alone or in the presence of **1a** was ~7 kcal/mol, indicating a remarkable stabilization of the G-4 conformation upon drug binding.

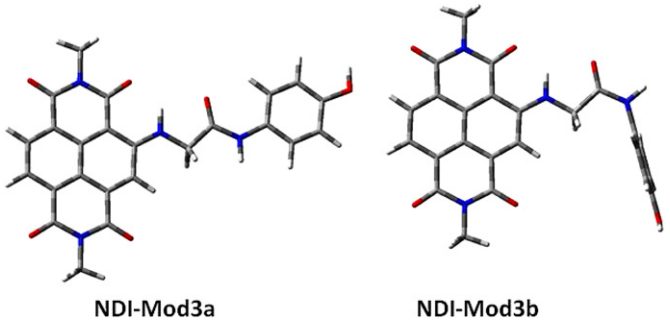

Fig. 2. Geometries of the conformations for the model NDI-Mod3, located at B3LYP/6-31G + G(d,p) level of theory.

Table 1
Relative energies (in kcal/mol) of the two conformers NDI-Mod3a and NDI-Mod3b computed at DFT level of theory.

Model	Relative energy in gas phase		Relative free energy in aqueous solvent	
	A	B	C	D
NDI-Mod3a	0.00	0.00	0.00	0.00
NDI-Mod3b	+1.96	+1.43	+5.57	+5.31

A: Geometries optimized in gas phase at B3LYP/6-31G(d) level of theory. **B:** Geometries optimized in gas phase at B3LYP/6-31 + G(d,p) level of theory. **C**: Geometries optimized in aqueous solution at PCM-B3LYP/6-31G(d) level of theory, using UHF radii. **D**: Computed in gas aqueous solution by single-point calculation at PCM-B3LYP/6-31 + G(d,p) level of theory, on gas phase optimized structures, using UAHF radii.

Table 2
$\Delta T_{1/2}$ of reversible binding NDI compounds measured by FRET of the labelled oligonucleotide F21T in K^+ solution in the absence or presence of competitor DNAs.

NDI	$\Delta T_{1/2}$/°C				
	1.0 μM	1:1 27NHEG:F21T	10:1 27NHEG:F21T	1:1 dsDNA:F21T	10:1 dsDNA:F21T
1a	20.9 ± 0.3	7.0 ± 0.5 (65%)	1.0 ± 0.1 (95%)	17.0 ± 0.3 (15%)	8.0 ± 0.5 (60%)
2a	15.9 ± 0.6	5.0 ± 0.3 (68%)	1.0 ± 0.2 (94%)	14.0 ± 0.8 (65%)	7.0 ± 0.3 (55%)
3a	14.0 ± 0.4				
4a	11.9 ± 0.4				
NDI-AminoPhenol	18.2 ± 0.3				

The stoichiometry of 4GGG/**1a** complex was analyzed by incubating 4GGG DNA with increasing molar ratios of NDI and analyzing samples by CD spectroscopy. As shown in Fig. 3C, **1a** reached binding saturation at 3:1 drug:DNA molar ratio. The ellipticity versus molar ratio plot for the binding of **1a** to 4GGG DNA, obtained from the CD titration data, indicates a biphasic behaviour: at ratios below 1 extrapolation of the linear portion (dashed-line) to a ratio of 2 suggests the initial onset of a ligand:DNA 2:1 complex, while for ratios between 1 and 3 further interaction is evidenced. Above a molar ratio of 3, no substantial change in ellipticity occurs. These data are consistent with the formation of two major types of complex (NDI:DNA 2:1 and 3:1), both characterized by remarkably high affinity constants.

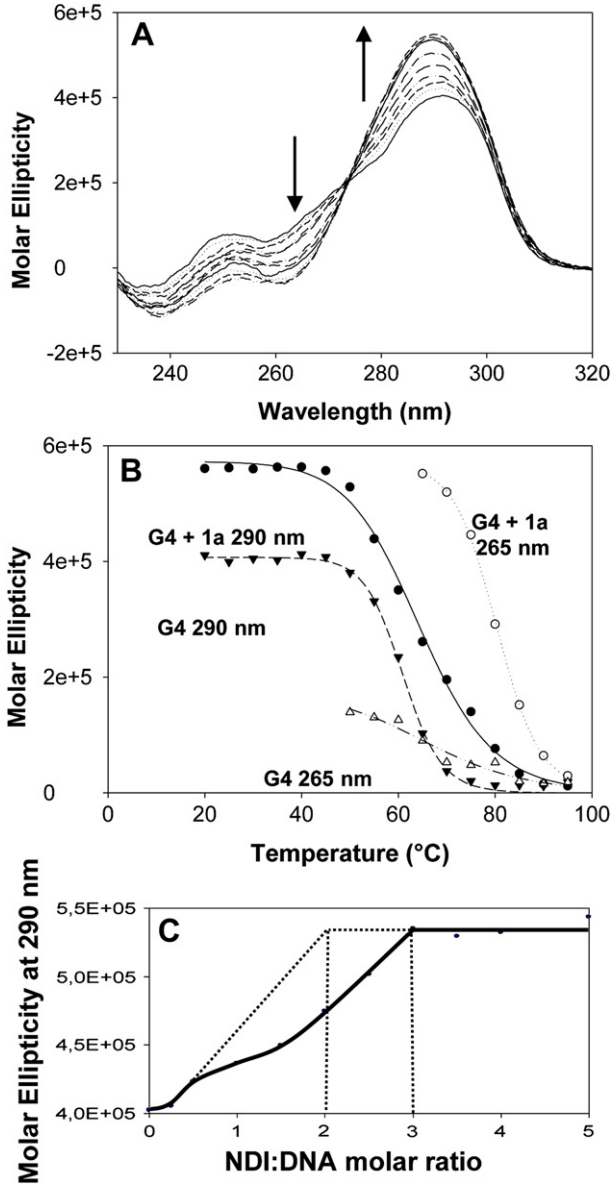

Fig. 3. CD analysis of 4GGG DNA in the presence of **1a**. A) 4GGG was incubated with increasing molar ratio of NDI (0, 0.25, 0.5, 1.0, 1.5, 2.0, 2.5, 3.0, 3.5, 4.0, 5.0, 6.0) and spectra were recorded at 20 °C. B) 4GGG was incubated either alone or in the presence of **1a** (4:1 NDI:DNA) and spectra were recorded at increasing temperatures (20–95 °C). Molar ellipticity values at 290 nm and 265 nm were plotted against temperature. C) Molar ellipticity values at 290 nm were plotted against different NDI:DNA molar ratios.

3.6. Alkylating NDI derivatives selectively alkylate G-quadruplex folded DNA

Alkylating NDI-QMPs present an additional hydroxymethyl moiety on the phenol group of the side chain. As such, they are QMP and they can be activated by mild heating (40 °C), compatible with physiological treatment.

To check that the introduction of the new chemical function did not impair efficient reversible ligand interaction with telomeric DNA, the ability of **1** to retain G-4 stabilization was assessed by CD analysis. As shown in Fig. 4, incubation of **1** with 4GGG DNA at 20 °C induced an increase in the peak at 290 nm and a slight decrease in the peak at 265 nm, similarly to its non-alkylating analogue, **1a**. However, when **1** and **1a** were incubated with the telomeric oligonucleotide at 40 °C for 24 h (alkylating conditions for **1**), both CD spectra presented a much more pronounced shoulder at 265 nm and a more intense negative peak at 240 nm (Fig. 4), indicating that a) alkylation does not impair/modify G-4 conformation and b) a different G-4 conformation is prevalently stabilized by both compounds at temperatures close to physiological. To note that 4GGG did not show CD spectral variation between 20° and 40 °C.

Additionally, reversible binding properties towards 4GGG DNA was evaluated for compound **1** and **1a** by surface plasmon resonance (SPR) at 25 °C. K_d values for compounds **1** and **1a** were

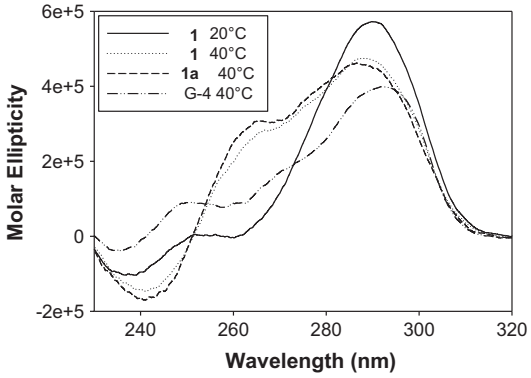

Fig. 4. CD analysis of 4GGG DNA in the presence of **1**. 4GGG either alone or in the presence of **1** NDI (4:1 NDI:DNA) was incubated for 24 h at 20 °C or 40 °C before spectra measurement. **1a** was used as a non-alkylating control to check the alkylation effect of **1** on telomeric DNA when treated at 40 °C.

$(8.9 \pm 2.6) \times 10^{-8}$ M and $(1.45 \pm 0.29) \times 10^{-7}$ M, respectively, indicating that the introduction of the QMP into the NDI template did not impair target recognition properties (Fig. 2S, Supporting information).

The ability of the alkylating NDIs to attack the 4GGG folded DNA was next assessed by denaturing gel electrophoresis. Increasing NDI amounts (30 nM–10 μM) were incubated at 40 °C for 24 h with the ^{32}P-labelled 4GGG oligonucleotide. Controls for the highest NDI concentration incubated with DNA at 4 °C were included. Compounds **1a** and **2a** were used as non-alkylating control molecules. As shown in Fig. 5A and B, alkylation was assessed by the formation of two bands migrating slower than the full length oligonucleotide.

Both in the H- and Br-alkylating NDI series, $n = 1$ compounds (**1** and **2**) were the best alkylating agents, where the sum of the two alkylation adducts obtained at 10 μM NDI concentration reached 16.8% and 12.8% for **1** and **2**, respectively, over total DNA amount (Fig. 5C).

In particular, both compounds induced a faster migrating alkylation band even at the lowest tested NDI concentration (i.e. 30 nM, lanes 3, Fig. 5A and B). At higher drug amounts (starting from 1.2 μM, lanes 5, Fig. 5A and B), a second slower migrating alkylation band appeared and increased over NDI concentration. Contrary, control reversible NDIs did not show any alkylation band. Based on this behaviour and on previous results [43,47–49], it is plausible that the faster and slower migrating alkylation bands correspond to 1:1 and 2:1 NDI:DNA adducts, respectively. We have shown above that 3 NDI molecules can reversibly bind the G-4 telomeric structure; here we find that 1 or 2 ligand molecules can covalently bind the G-4 DNA. Therefore, we suggest that only 2 NDI

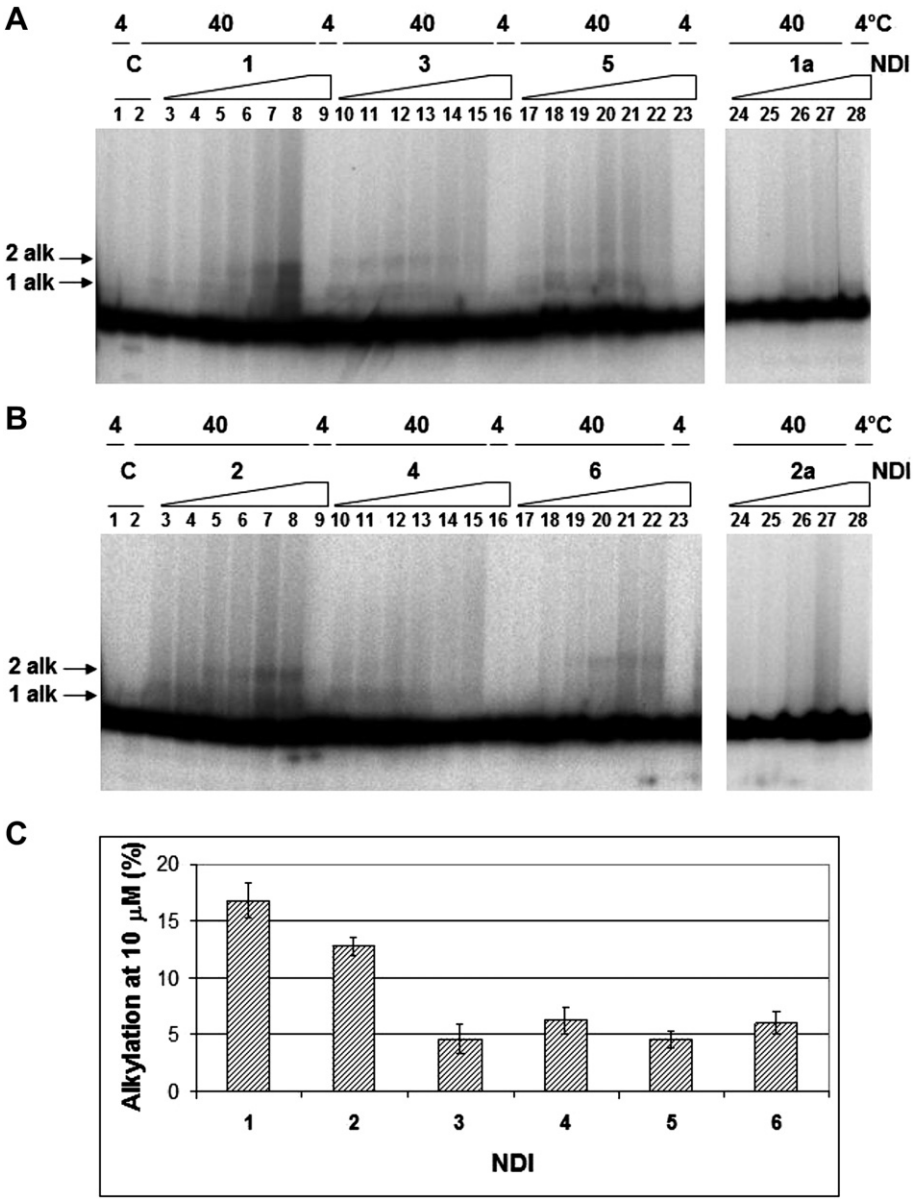

Fig. 5. Alkylation effects of **1** NDI on 4GGG DNA. A) Increasing amounts of compounds **1**, **3** and **5** along with **1a** as non-alkylating control and B) **2**, **4** and **6** along with **2a** as non-alkylating control (30 nM–10 μM) were incubated with the ^{32}P-labelled 4GGG DNA at 40 °C for 24 h. Reaction samples were run on a 20% denaturing polyacrylamide gel and visualized by phosphorimaging. 1alk and 2alk stand for first (faster migrating) and second (slower migrating) alkylation adduct, respectively. Control lanes are referred as C and are 4GGG DNA incubated at 4 °C (lane 1) or 40 °C (lane 2) without the compounds. C) Quantification of alkylation band amounts obtained at 10 μM for all compounds. Quantifications were performed by three different operators and reported are mean values with standard deviations.

molecules in the reversible complex with G-4 are appropriately positioned to mediate the successive covalent attack (i.e. loops), while the third NDI molecule is bound in such a location where the QM arm cannot reach a close suitable nucleophilic site (i.e. groove). Between **1** and **2**, the former was more efficient in inducing alkylation (Fig. 5C). Compounds **3**, **4**, **5** and **6** were also able to alkylate G-4 DNA at low drug concentration; however alkylation rate did not increase over concentration. It is possible that precipitation occurred at higher drug amounts.

Selectivity of **1** was assessed by incubating increasing NDI amounts (12 nM–50 μM) with 4GGG, ss-scrambled DNA (a single-stranded scrambled 4GGG DNA whose sequence base composition, but not order, corresponded to that of 4GGG oligo), and ds-scrambled DNA (ssDNA and its complementary sequence). As shown in Fig. 6, **1** was able to alkylate G-4 DNA even at 12 nM (lane 3), while with ss-scrambled DNA no clear alkylation band was readily appreciable; however a smeared band was detectable from 780 nM (lane 6, ss). Finally, alkylation towards ds-scrambled DNA was very modest and appreciable starting from 12.5 μM (lane 8, ds). Hence **1** was 100–1000 times more selective for G-4 DNA versus different conformations adopted by single-stranded and double-stranded oligonucleotides, respectively. Compound **2** yielded similar results (data not shown).

Finally, the site of alkylation was investigated by enzymatic digestion. The slowest migrating band in Fig. 5, alk2, was gel-purified and subjected to digestion with exonuclease I (exoI), which catalyzes the removal of nucleotides from single-stranded-DNA in the 3′ to 5′ direction. As shown in Fig. 7, the purified adduct was slightly unstable: in fact, from alk2 a 10–20% of alk1 (see Fig. 5) and non-alkylated oligonucleotides re-formed. However, this behaviour is not unexpected for alkylation adducts generated from electron rich QMs. In fact, only the covalent adducts at the exocyclic NH_2 groups of C, G and A moieties are thermodynamically stable, and alkylation adducts at different sites should revert to free QM and DNA. Given this initial consideration, the exoI enzyme cut the control non-alkylated 4GGG all throughout the sequence and presented a major slow-down region at the level of the first loop (A7, starting from the 5′-end, indicated by the dashed-line arrow in Fig. 7). In contrast, the alk2 purified sample presented two major slow-down regions at the level of the second and third G repeats (G9–G10 and G15–G16, indicated by the continuous-line arrows in Fig. 7), which can be accounted for NDI putative alkylation sites. Alk1 and Alk2 characterization by MS is still under investigation.

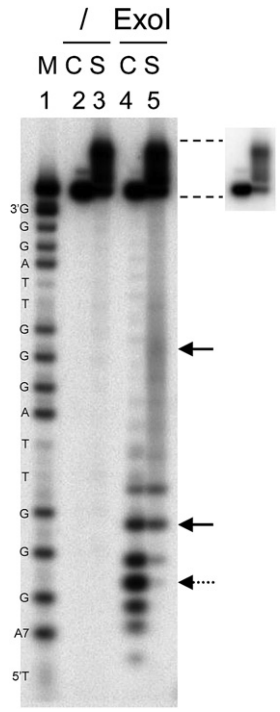

Fig. 7. ExoI digestion of the slower migrating adduct of compound **1** with 4GGG DNA. NDI 1/4GGG adduct was gel-purified, digested with ExoI, run on a 20% denaturing polyacrylamide gel and visualized by phosphorimaging. The non-alkylated 4GGG DNA was gel-purified and treated in the same condition as a control. Continuous-line arrows indicate the major slow-down sites (putative alkylation sites) in the purified adduct. The dashed-line arrow indicate the major slow-down site in the control non-alkylated G-4 DNA. The upper-right image shows a shorter acquisition of the non-digested DNA signals.

Alkylating NDIs are More Cytototoxic Against Telomerase-positive Cell Lines. The effect of the NDI derivatives against two telomerase-positive human carcinoma cell lines (lung and colon) was investigated. As shown in Table 3, both alkylating and non-alkylating NDIs **1**, **1a**, **2** and **2a** were cytotoxic in the low micromolar range. In general, all NDIs were more active against the colon than the lung cell line, and **1**-derived compounds were more active than **2**-derived NDIs, which parallel the alkylation/binding

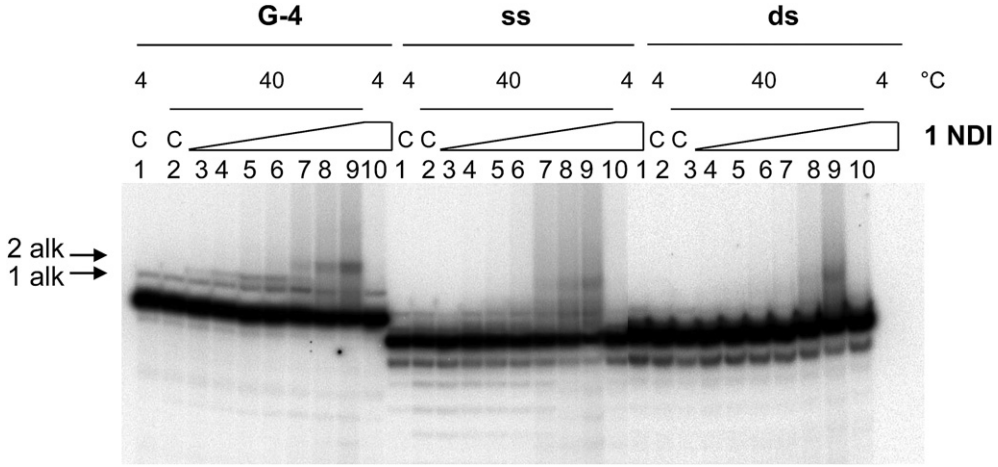

Fig. 6. Selectivity of **1** NDI towards DNA conformations. Increasing amounts (12 nM–50 μM) of **1** NDI was incubated at 40 °C for 24 h with the G-4 conformed 4GGG DNA, and with 4GGG scrambled single- and double-stranded oligonucleotides whose base composition but not sequence corresponded to that of 4GGG DNA. Samples were run on a 20% denaturing polyacrylamide gel and visualized by phosphorimaging. 1alk and 2alk stand for first (faster migrating) and second (slower migrating) alkylation adduct, respectively.

Table 3
Cytotoxicity of NDIs **1** and **2** towards telomerase-positive carcinoma cell lines (Lung, A549, and Colon, HT-29) and telomerase-negative Human Foreskin Fibroblast (HHF) at 48 h.

NDIs	EC_{50} (μM) HT-29	EC_{50} (μM) A549	EC_{50} (μM) HFF
	Telomerase+	Telomerase+	Telomerase−
1	4.5 ± 1.9	5.5 ± 1.3	18 ± 3
1a	1.4 ± 0.5	4.5 ± 0.6	18 ± 3
2	4.2 ± 0.6	20.6 ± 3.2	40 ± 5
2a	9.3 ± 2.2	27.5 ± 5.0	40 ± 5

efficiency against G-4 DNA, which is higher for compounds **1**/**1a**. Interestingly, NDI cytotoxicity against telomerase-negative human foreskin fibroblasts (HFF) was 2–10 times lower, indicating a moderate effect on telomeres. Disappointingly, no striking different effect was observed between alkylating and non-alkylating compounds, which could partially be ascribed to the low efficiency of the alkylation event. This aspect suggests the direction for the development of future hybrid ligand-alkylating agents, which should exhibit higher alkylating efficiency.

4. Conclusions

A new small library of tri-substituted NDI derivatives has been prepared and tested towards G-4 folded DNA. These molecules have been chemically engineered to embed an alkylating quinone methide precursor (QMP), whose reactivity has been triggered by mild thermal digestion ($T = 40$ °C). Substituents on the alkylating moiety play a dynamical role influencing both the ligand conformational flexibility and the reactivity of the alkylating agent precursor.

The separate analysis of the reversible and irreversible binding properties showed that these NDIs are good ligands of G-4 telomeric DNA (**1a**–**4a**), with a promising duplex vs quadruplex selectivity. It is worthy to underline that the introduction of the amido functional group in the ligand structure strongly modifies the interaction properties of these compounds towards the G-4 folded DNA and its ligand:DNA molecular ratio. In addition, the semi-rigid amido spacer in NDIs **1a** and **2a** appears to be a crucial feature improving G-4 reversible binding properties, by conferring planarity to the whole ligand structure.

Addition of alkylating moiety to NDIs **1**–**6**, does not impair their good recognition properties towards the G-4 folded DNA. Alkylation by NDIs **1** and **2** results particularly efficient against G-4 folded DNA structures, whilst negligible alkylation has been observed towards double-stranded-DNA. The tested NDIs were found active against two telomerase-positive cancer cell lines; in general, NDIs showed less short-term cytotoxicity than classic anticancer drugs (i.e. doxorubicin, paclitaxel), suggesting that their activity may be mediated by a more specific telomerase/telomere-oriented mechanism of action. Therefore, these new compounds represent promising selective telomeric G-4 alkylating agents endowed with anticancer activity.

Due to the deep structural and environmental modifications induced by alkylation on G-4 structures, we strongly believe that designing chemically dynamic G-4 ligands, as the above described NDI derivatives, could represent a useful tool for unravelling G-4 sensitive tumorigenic pathways.

Acknowledgements

This work was supported by MIUR, Grant FIRB-Ideas RBID082ATK, Grants AIRC 5826 and 8861 (Associazione Italiana per la Ricerca sul Cancro) and by Pavia University.

Appendix. Supporting information

Supporting information related to this article can be found online at doi:10.1016/j.biochi.2011.06.015.

References

[1] J.T. Davis, G-quartets 40 years later: from 5′-GMP to molecular biology and supramolecular chemistry, Angew. Chem. Int. Ed. Engl. 43 (2004) 668–698.
[2] M. Gellert, M.N. Lipsett, D.R. Davies, Helix formation by guanylic acid, Proc. Natl. Acad. Sci. 48 (1962) 2013–2018.
[3] D.E. Gilbert, J. Feigon, Multistranded DNA structures, Curr. Opin. Struct. Biol. 9 (1999) 305–314.
[4] J. Suhnel, Beyond nucleic acid base pairs: from triads to heptads, Biopolymers 61 (2001) 32–51.
[5] T. Simonsson, G-quadruplex DNA structures-variations on a theme, Biol. Chem. 382 (2001) 621–628.
[6] S. Burge, G.N. Parkinson, P. Hazel, A.K. Todd, S. Neidle, Quadruplex DNA: sequence, topology and structure, Nucleic Acids Res. 34 (2006) 5402–5415.
[7] P.H. Wanrooij, J.P. Uhler, T. Simonsson, M. Falkenberg, C.M. Gustafsson, G-quadruplex structures in RNA stimulate mitochondrial transcription termination and primer formation, Proc. Natl. Acad. Sci. USA 107 (2010) 16072–16077.
[8] T. Agarwal, S. Roy, T.K. Chakraborty, S. Maiti, Furan based cyclic homo-oligopeptides bind G-quadruplex selectively and repress c-MYC transcription, Bioorg. Med. Chem. Lett. 20 (2010) 4346–4349.
[9] X.D. Wang, T.M. Ou, Y.J. Lu, Z. Li, Z. Xu, C. Xi, J.H. Tan, S.L. Huang, L.K. An, D. Li, Turning off transcription of the bcl-2 gene by stabilizing the bcl-2 promoter quadruplex with quindoline derivatives, J. Med. Chem. 53 (2010) 4390–4398.
[10] L.E. Xodo, M. Paramasivam, A. Membrino, S. Cogoi, Protein hnRNPA1 binds to a critical G-rich element of KRAS and unwinds G-quadruplex structures: implications in transcription, Nucleic Acids Symp. Ser. (Oxf.) 52 (2008) 159–160.
[11] C. Arnal-Herault, A. Banu, M. Barboiu, M. Michau, A. van der Lee, Amplification and transcription of the dynamic supramolecular chirality of the guanine quadruplex, Angew. Chem. Int. Ed. Engl. 46 (2007) 4268–4272.
[12] S. Cogoi, L.E. Xodo, G-quadruplex formation within the promoter of the KRAS proto-oncogene and its effect on transcription, Nucleic Acids Res. 34 (2006) 2536–2549.
[13] A. Siddiqui-Jain, C.L. Grand, D.J. Bearss, L.H. Hurley, Direct evidence for a G-quadruplex in a promoter region and its targeting with a small molecule to repress c-MYC transcription, Proc. Natl. Acad. Sci. USA 99 (2002) 11593–11598.
[14] S.L. Palumbo, S.W. Ebbinghaus, L.H. Hurley, Formation of a unique end-to-end stacked pair of G-quadruplexes in the hTERT core promoter with implications for inhibition of telomerase by G-quadruplex-interactive ligands, J. Am. Chem. Soc. 131 (2009) 10878–10891.
[15] A.K. Todd, S. Neidle, The relationship of potential G-quadruplex sequences in cis-upstream regions of the human genome to SP1-binding elements, Nucleic Acids Res. 36 (2008) 2700–2704.
[16] R. Rodriguez, S. Muller, J.A. Yeoman, C. Trentesaux, J.F. Riou, S. Balasubramanian, A novel small molecule that alters shelterin integrity and triggers a DNA-damage response at telomeres, J. Am. Chem. Soc. 130 (2008) 15758–15759.
[17] A. Rangan, O.Y. Fedoroff, L.H. Hurley, Induction of duplex to G-quadruplex transition in the c-myc promoter region by a small molecule, J. Biol. Chem. 276 (2001) 4640–4646.
[18] K.I. McLuckie, Z.A. Waller, D.A. Sanders, D. Alves, R. Rodriguez, J. Dash, G.J. McKenzie, A.R. Venkitaraman, S. Balasubramanian, G-Quadruplex-binding benzo[a]phenoxazines down-regulate c-KIT expression in human gastric carcinoma cells, J. Am. Chem. Soc. 133 (2011) 2658–2663.
[19] S.T. Hsu, P. Varnai, A. Bugaut, A.P. Reszka, S. Neidle, S. Balasubramanian, A G-rich sequence within the c-kit oncogene promoter forms a parallel G-quadruplex having asymmetric G-tetrad dynamics, J. Am. Chem. Soc. 131 (2009) 13399–13409.
[20] H. Fernando, A.P. Reszka, J. Huppert, S. Ladame, S. Rankin, A.R. Venkitaraman, S. Neidle, S. Balasubramanian, A conserved quadruplex motif located in a transcription activation site of the human c-kit oncogene, Biochemistry 45 (2006) 7854–7860.
[21] S. Rankin, A.P. Reszka, J. Huppert, M. Zloh, G.N. Parkinson, A.K. Todd, S. Ladame, S. Balasubramanian, S. Neidle, Putative DNA quadruplex formation within the human c-kit oncogene, J. Am. Chem. Soc. 127 (2005) 10584–10589.
[22] H. Li, Y. Liu, S. Lin, G. Yuan, Spectroscopy probing of the formation, recognition, and conversion of a G-quadruplex in the promoter region of the bcl-2 oncogene, Chem. Eur. J. 15 (2009) 2445–2452.
[23] J. Dai, T.S. Dexheimer, D. Chen, M. Carver, A. Ambrus, R.A. Jones, D. Yang, An intramolecular G-quadruplex structure with mixed parallel/antiparallel G-strands formed in the human BCL-2 promoter region in solution, J. Am. Chem. Soc. 128 (2006) 1096–1098.
[24] C. Douarre, D. Gomez, H. Morjani, J.M. Zahm, M.F. O'Donohue, L. Eddabra, P. Mailliet, J.F. Riou, C. Trentesaux, Overexpression of Bcl-2 is associated with apoptotic resistance to the G-quadruplex ligand 12459 but is not sufficient to

confer resistance to long-term senescence, Nucleic Acids Res. 33 (2005) 2192–2203.
[25] J.W. Shay, W.E. Wright, Telomerase therapeutics for cancer: challenges and new directions, Nat. Rev. Drug Discov. 5 (2006) 577–584.
[26] R. Shahid, A. Bugaut, S. Balasubramanian, The BCL-2 5′ untranslated region contains an RNA G-quadruplex-forming motif that modulates protein expression, Biochemistry 49 (2010) 8300–8306.
[27] A. Arola, R. Vilar, Stabilisation of G-quadruplex DNA by small molecules, Curr. Top. Med. Chem. 8 (2008) 1405–1415.
[28] D. Monchaud, M.P. Teulade-Fichou, A hitchhiker's guide to G-quadruplex ligands, Org. Biomol. Chem. 6 (2008) 627–636.
[29] A.M. Burger, F. Dai, C.M. Schultes, A.P. Reszka, M.J. Moore, J.A. Double, S. Neidle, The G-quadruplex-interactive molecule BRACO-19 inhibits tumor growth, consistent with telomere targeting and interference with telomerase function, Cancer Res. 65 (2005) 1489–1496.
[30] S. Sparapani, S.M. Haider, F. Doria, M. Gunaratnam, S. Neidle, Rational design of acridine-based ligands with selectivity for human telomeric quadruplexes, J. Am. Chem. Soc. 132 (2010) 12263–12272.
[31] A. De Cian, E. Delemos, J.L. Mergny, M.P. Teulade-Fichou, D. Monchaud, Highly efficient G-quadruplex recognition by bisquinolinium compounds, J. Am. Chem. Soc. 129 (2007) 1856–1857.
[32] P. Yang, A. De Cian, M.P. Teulade-Fichou, J.L. Mergny, D. Monchaud, Engineering bisquinolinium/thiazole orange conjugates for fluorescent sensing of G-quadruplex DNA, Angew. Chem. Int. Ed. Engl. 48 (2009) 2188–2191.
[33] M.Y. Kim, H. Vankayalapati, K. Shin-Ya, K. Wierzba, L.H. Hurley, Telomestatin, a potent telomerase inhibitor that interacts quite specifically with the human telomeric intramolecular g-quadruplex, J. Am. Chem. Soc. 124 (2002) 2098–2099.
[34] M. Tera, H. Ishizuka, M. Takagi, M. Suganuma, K. Shin-ya, K. Nagasawa, Macrocyclic hexaoxazoles as sequence- and mode-selective G-quadruplex binders, Angew. Chem. Int. Ed. Engl. 47 (2008) 5557–5560.
[35] C. Sissi, L. Lucatello, A. Paul Krapcho, D.J. Maloney, M.B. Boxer, M.V. Camarasa, G. Pezzoni, E. Menta, M. Palumbo, Tri-, tetra- and heptacyclic perylene analogues as new potential antineoplastic agents based on DNA telomerase inhibition, Bioorg. Med. Chem. 15 (2007) 555–562.
[36] F. Cuenca, O. Greciano, M. Gunaratnam, S. Haider, D. Munnur, R. Nanjunda, W.D. Wilson, S. Neidle, Tri- and tetra-substituted naphthalene diimides as potent G-quadruplex ligands, Bioorg. Med. Chem. Lett. 18 (2008) 1668–1673.
[37] M. Gunaratnam, S. Swank, S.M. Haider, K. Galesa, A.P. Reszka, M. Beltran, F. Cuenca, J.A. Fletcher, S. Neidle, Targeting human gastrointestinal stromal tumor cells with a quadruplex-binding small molecule, J. Med. Chem. 52 (2009) 3774–3783.
[38] G. Collie, A.P. Reszka, S.M. Haider, V. Gabelica, G.N. Parkinson, S. Neidle, Selectivity in small molecule binding to human telomeric RNA and DNA quadruplexes, Chem. Commun. 48 (2009) 7482–7484.
[39] S.M. Hampel, A. Sidibe, M. Gunaratnam, J.F. Riou, S. Neidle, Tetrasubstituted naphthalene diimide ligands with selectivity for telomeric G-quadruplexes and cancer cells, Bioorg. Med. Chem. Lett. 20 (2010) 6459–6463.
[40] E. Modica, R. Zanaletti, M. Freccero, M. Mella, Alkylation of amino acids and glutathione in water by o-quinone methide. Reactivity and selectivity, J. Org. Chem. 66 (2001) 41–52.
[41] C. Di Valentin, M. Freccero, R. Zanaletti, M. Sarzi-Amade, o-Quinone methide as alkylating agent of nitrogen, oxygen, and sulfur nucleophiles. The role of H-bonding and solvent effects on the reactivity through a DFT computational study, J. Am. Chem. Soc. 123 (2001) 8366–8377.
[42] M. Freccero, C. Di Valentin, M. Sarzi-Amade, Modeling H-bonding and solvent effects in the alkylation of pyrimidine bases by a prototype quinone methide: a DFT study, J. Am. Chem. Soc. 125 (2003) 3544–3553.
[43] M. Di Antonio, F. Doria, S.N. Richter, C. Bertipaglia, M. Mella, C. Sissi, M. Palumbo, M. Freccero, Quinone methides tethered to naphthalene diimides as selective G-quadruplex alkylating agents, J. Am. Chem. Soc. 131 (2009) 13132–13141.
[44] M. Di Antonio, F. Doria, M. Mella, D. Merli, A. Profumo, M. Freccero, Novel naphthalene diimides as activatable precursors of bisalkylating agents, by reduction and base catalysis, J. Org. Chem. 72 (2007) 8354–8360.
[45] E.E. Weinert, R. Dondi, S. Colloredo-Melz, K.N. Frankenfield, C.H. Mitchell, M. Freccero, S.E. Rokita, Substituents on quinone methides strongly modulate formation and stability of their nucleophilic adducts, J. Am. Chem. Soc. 128 (2006) 11940–11947.
[46] M. Freccero, R. Gandolfi, M. Sarzi-Amade, Selectivity of purine alkylation by a quinone methide. Kinetic or thermodynamic control? J. Org. Chem. 68 (2003) 6411–6423.
[47] D. Verga, M. Nadai, F. Doria, C. Percivalle, M. Di Antonio, M. Palumbo, S.N. Richter, M. Freccero, Photogeneration and reactivity of naphthoquinone methides as purine selective DNA alkylating agents, J. Am. Chem. Soc. 132 (2010) 14625–14637.
[48] D. Verga, S.N. Richter, M. Palumbo, R. Gandolfi, M. Freccero, Bipyridyl ligands as photoactivatable mono- and bis-alkylating agents capable of DNA cross-linking, Org. Biomol. Chem. 5 (2007) 233–235.
[49] F. Doria, S.N. Richter, M. Nadai, S. Colloredo-Mels, M. Mella, M. Palumbo, M. Freccero, BINOL-amino acid conjugates as triggerable carriers of DNA-targeted potent photocytotoxic agents, J. Med. Chem. 50 (2007) 6570–6579.
[50] S. Colloredo-Mels, F. Doria, D. Verga, M. Freccero, Photogenerated quinone methides as useful intermediates in the synthesis of chiral BINOL ligands, J. Org. Chem. 71 (2006) 3889–3895.
[51] (a) S.N. Richter, S. Maggi, S.C. Mels, M. Palumbo, M. Freccero, Binol quinone methides as bisalkylating and DNA cross-linking agents, J. Am. Chem. Soc. 126 (2004) 13973–13979;
(b) C. Percivalle, A. La Rosa, D. Verga, F. Doria, M. Mella, M. Palumbo, M. Di Antonio, M. Freccero, Quinone methide generation via photoinduced electron transfer, J. Org. Chem. 76 (2011) 3096–3106.
[52] F. Doria, M. Nadai, M. Di Antonio, R. Stocco, L. Germani, C. Percivalle, M. Petenzi, D. Verga, C. Sissi, N. Zaffaroni, M. Folini, G. Cimino-Reale, M. Palumbo, S.N. Richter, M. Freccero, Hybrid ligand/alkylating agents targeting telomeric G-quadruplex structures, Chem. Biol., submitted for publication.
[53] F. Doria, M. Di Antonio, M. Benotti, D. Verga, M. Freccero, Substituted heterocyclic naphthalene diimides with unexpected acidity. Synthesis, properties, and reactivity, J. Org. Chem. 74 (2009) 8616–8625.
[54] M.J. Frisch, G.W. Trucks, H.B. Schlegel, G.E. Scuseria, M.A. Robb, J.R. Cheeseman, J.A. Montgomery Jr., T. Vreven, K.N. Kudin, J.C. Burant, J.M. Millam, S.S. Iyengar, J. Tomasi, V. Barone, B. Mennucci, M. Cossi, G. Scalmani, N. Rega, G.A. Petersson, H. Nakatsuji, M. Hada, M. Ehara, K. Toyota, R. Fukuda, J. Hasegawa, M. Ishida, T. Nakajima, Y. Honda, O. Kitao, H. Nakai, M. Klene, X. Li, J.E. Knox, H.P. Hratchian, J.B. Cross, C. Adamo, J. Jaramillo, R. Gomperts, R.E. Stratmann, O. Yazyev, A.J. Austin, R. Cammi, C. Pomelli, J.W. Ochterski, P.Y. Ayala, K. Morokuma, G.A. Voth, P. Salvador, J.J. Dannenberg, V.G. Zakrzewski, S. Dapprich, A.D. Daniels, M.C. Strain, O. Farkas, D.K. Malick, A.D. Rabuck, K. Raghavachari, J.B. Foresman, J.V. Ortiz, Q. Cui, A.G. Baboul, S. Clifford, J. Cioslowski, B.B. Stefanov, G. Liu, A. Liashenko, P. Piskorz, I. Komaromi, R.L. Martin, D.J. Fox, T. Keith, M.A. Al-Laham, C.Y. Peng, A. Nanayakkara, M. Challacombe, P.M.W. Gill, B. Johnson, W. Chen, M.W. Wong, C. Gonzalez, J.A. Pople, Wallingford CT, Gaussian 03, Revision C.02. Gaussian, Inc., 2004.
[55] J.E. Del Bene, W.B. Person, K. Szczepaniak, Properties of hydrogen-bonded complexes obtained from the B3LYP functional with 6-31G(d,p) and 6-31+G(d,p) basis-sets: comparison with MP2/6-31+G(d,p) results and experimental-data. J. Phys. Chem. 99 (1995) 10705–10707.
[56] V. Barone, M. Cossi, J. Tomasi, A new definition of cavities for the computation of solvation free energies by the polarizable continuum model, J. Chem. Phys. 107 (1997) 3210–3221.
[57] N.J. Greenfield, Using circular dichroism collected as a function of temperature to determine the thermodynamics of protein unfolding and binding interactions, Nat. Protoc. 1 (2006) 2527–2535.
[58] A. De Cian, L. Guittat, M. Kaiser, B. Saccà, S. Amrane, A. Bourdoncle, P. Alberti, M.P. Teulade-Fichou, L. Lacroix, J.L. Mergny, Fluorescence-based melting assays for studying quadruplex ligands, Methods 42 (2007) 183–195.
[59] A. Ambrus, D. Chen, J. Dai, T. Bialis, R.A. Jones, D. Yang, Human telomeric sequence forms a hybrid-type intramolecular G-quadruplex structure with mixed parallel/antiparallel strands in potassium solution, Nucleic Acids Res. 34 (2006) 2723–2735.
[60] R.D. Gray, L. Petraccone, J.O. Trent, J.B. Chaires, Characterization of a K^+-induced conformational switch in a human telomeric DNA oligonucleotide using 2-aminopurine fluorescence, Biochemistry 49 (2010) 179–194.